NGU Report 2000.077

Interpretation of Magnetic Data, Eidangerfjord

NGU
Norges geologiske undersøkelse
Geological Survey of Norway
Geological Survey of Norway
N-7491 Trondheim, Norway
Tel.: 47 73 90 40 11
Telefax 47 73 92 16 20

REPORT

Report no.: 2000.077 | ISSN 0800-3416 | Grading: Åpen

Title:
Interpretation of Magnetic Data, Eidangerfjord

Authors:
Les P. Beard

Client:
Norcem AS

County:
Telemark

Commune:
Porsgrunn

Map-sheet name (M=1:250.000)
Skien

Map-sheet no. and -name (M=1:50.000)
1713 II Porsgrunn

Deposit name and grid-reference:

Number of pages: 40 Price (NOK): 105,-
Map enclosures:

Fieldwork carried out:	Date of report:	Project no.:	Person responsible:
09.1998, 04.2000	14.07.2000	2886.00	Jan S. Rønning

Summary:

Magnetic data from a 1998 NGU helicopter geophysical survey revealed a previously unknown magnetic lineament in the center of Eidangerfjord. The nature of the structure causing the magnetic anomaly could have consequences on carbonate mining operations beneath Eidangerfjord. Data from a 1988 seismic reflection survey over Eidangerfjord indicated the carbonate-igneous intrusive contact lies off the eastern boundary of the fjord. Analysis of magnetic data using Euler deconvolution, inversion for magnetic susceptibility, and combined forward and inverse modeling generally supports the contact location from the seismic survey. Modeling indicates the body causing the central fjord magnetic lineament is at least 200m wide and may cut into the carbonates. A large magnetic body, probably separate from the central fjord magnetic body, extends under the western side of the fjord. This western body may explain the high temperatures inferred from calcite grain coarsening in the carbonates.

Keywords: Geofysikk	Tolkning	Magnetometri
Prøvetaking	Karbonat	Larvikitt
Seismikk	Fagrapport	

CONTENTS

1 INTRODUCTION..... 4

2 GEOLOGICAL OVERVIEW..... 4

3 GEOPHYSICAL DATA AND MODELING..... 4

4 DISCUSSION AND CONCLUSIONS..... 23

5 ACKNOWLEDGMENTS..... 35

5 REFERENCES..... 35

6 APPENDIX..... 37

LIST OF FIGURES

Fig. 1. Eidangerfjord area map.
Fig. 2. Geology of Eidangerfjord area.
Fig. 3. Magnetic susceptibility data, Eidangerfjord.
Fig. 4. Q-values, Eidangerfjord.
Fig. 5. Euler deconvolution, SI = 0
Fig. 6. Euler deconvolution, SI = 1
Fig. 7. Estimated models from magnetic susceptibility inversion.
Fig. 8. Estimated models from combined inverse and forward modeling, 3 bodies.
Fig. 9. Estimated models from combined inverse and forward modeling, 3 bodies but with high Q central body.
Fig. 10. Estimated models from combined inverse and forward modeling, 2 bodies.
Fig. 11. Schematic drawing of geology beneath Eidangerfjord.
Fig. 12. Carbonate-larvikite contact.

1 INTRODUCTION

In September, 1998, a helicopter geophysical survey was carried out in the vicinity of Larvik. The westernmost portion of the survey area was flown over Eidangerfjord, Telemark (Fig. 1). Magnetic data from this survey revealed a subtle positive linear anomaly in the center of the fjord (Beard, 1999). Determining the nature of the structure causing this anomaly is important for carbonate mining operations taking place beneath the fjord near Brevik. If the magnetic anomaly represents a contact between the carbonates on the western side of the fjord and larvikites on the eastern side, then estimates of carbonate reserves will have to be revised downward, and estimated mine lifetime will be shorter. Similarly, if the central structure is not a contact, but represents a major obstacle to mining, this too will have an impact on estimating extraction costs. Based on seismic data, the contact has previously been estimated to lie close to the eastern side of the fjord (Noteby AS, 1988).

The magnetic data are examined in light of existing seismic, geological, and rock properties data. Forward and inverse magnetic modeling and Euler decomposition have been employed as tools to determine the nature of the structure causing the central magnetic anomaly, and to draw general conclusions on the geological structure beneath Eidangerfjord.

2 GEOLOGICAL OVERVIEW

For the purposes of magnetic modeling, the geological units in the vicinity of Eidangerfjord can be divided into two groups: magnetic rocks and non-magnetic rocks. The major exposed magnetic rocks are the igneous intrusives exposed on the eastern side of Eidangerfjord, part of the Oslo igneous province. These rocks consist mainly of larvikite and lardalite. The magnetic susceptibility of these rocks are typically 2 to 4 orders of magnitude higher than the rocks of sedimentary origin—carbonates, slate, and quartzite—exposed on the western side of the fjord. The other significant magnetic units in the area are the amphibolites and metagabbros exposed in Precambrian gneisses west from Brevik. These units and general geology of the Eidangerfjord area are shown in Fig. 2, taken from a subsection of the Skien 1:250 000 scale geological map compiled by Dons and Jorde (1976). The contact between the igneous rocks of the Oslo igneous province and sedimentary units to the west intersects Eidangerfjord at its northernmost point and continues along the fjord in a roughly N-S direction for 4-5 km before shifting to a NNW-SSE strike direction south from Brevik.

3 GEOPHYSICAL DATA AND MODELING

Magnetic data were collected in a 1998 NGU helicopter survey. The helicopter maintained a nominal flying height of 60m above ground level, flew at a speed of about 30 m/s. The

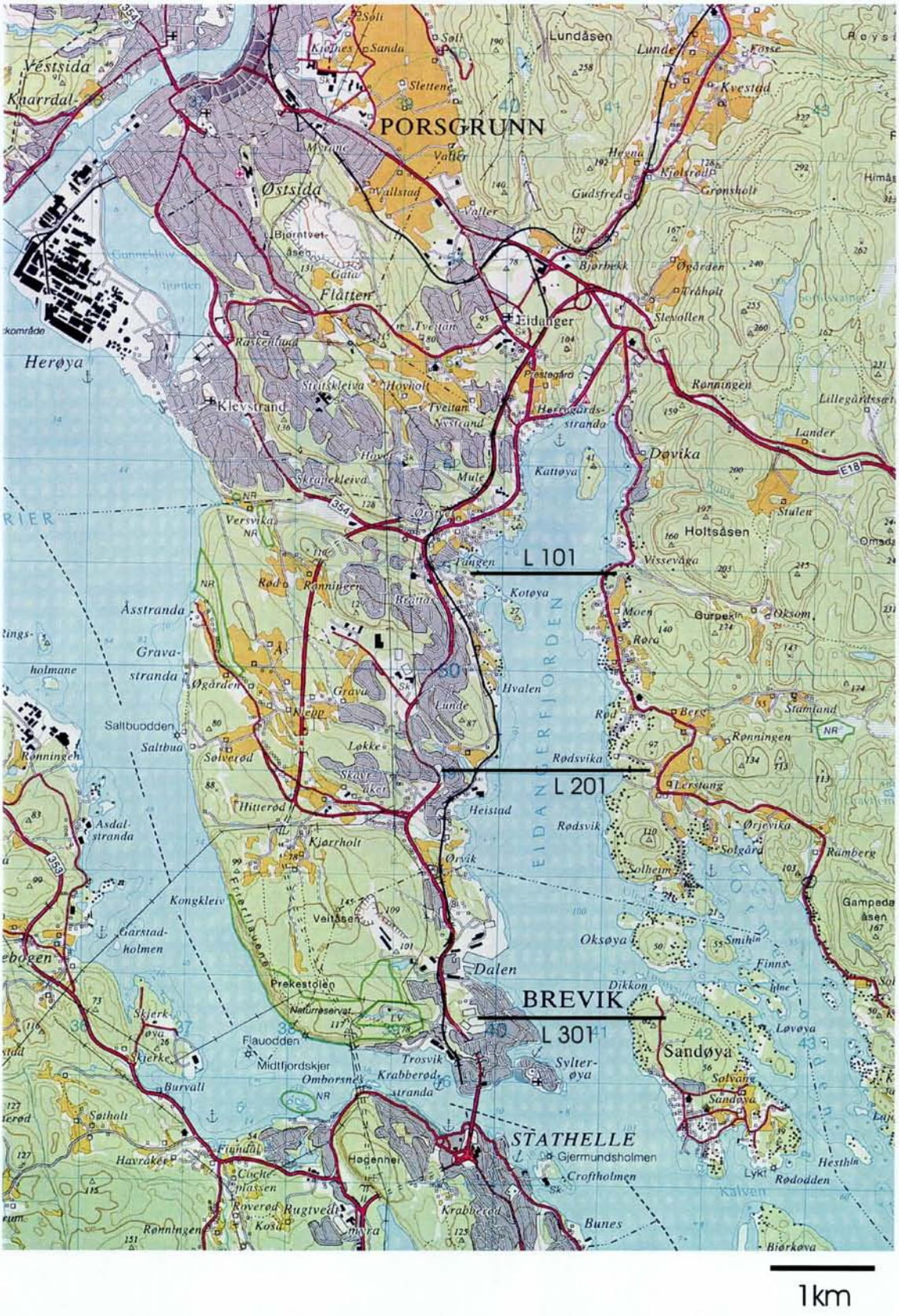

Fig. 1. Location map showing Eidangerfjord and the three cross-sections modeled in this report.

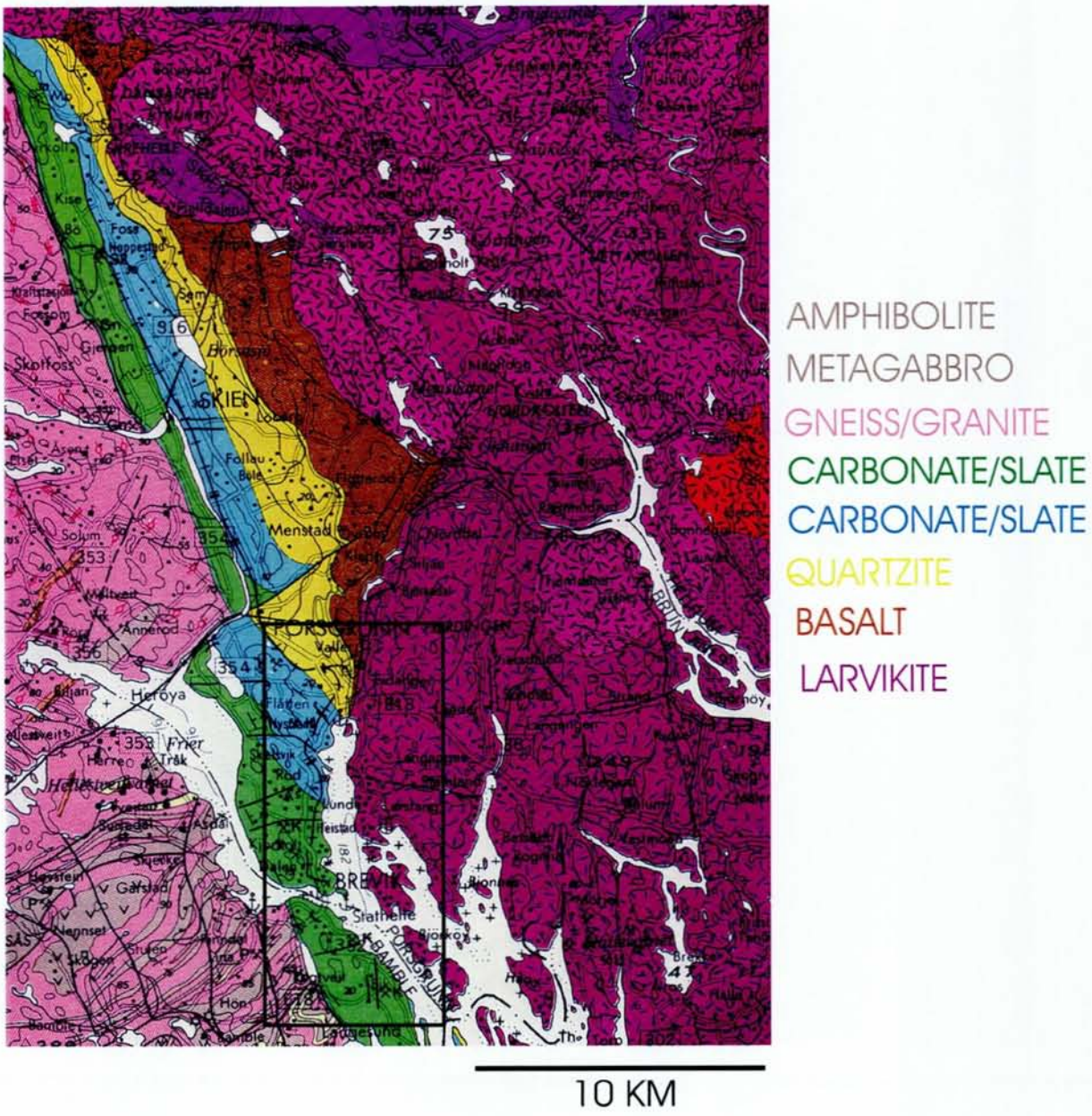

Fig. 2. Geology of the Eidangerfjord area. Eidangerfjord is centered in the rectangle. (After Dons and Jorde, 1976.)

magnetometer was suspended 15m below the helicopter, and so was 45 m above ground level. The magnetometer's sampling rate was 5 measurements per second. Diurnal variations in the magnetic field were estimated using a base magnetometer and these variations were removed from the raw magnetic data. The corrected data were then gridded and displayed in map form.

In this report, the magnetic data are analyzed using three different methods: Euler deconvolution, susceptibility estimation via automatic inversion, and combined forward and inverse modeling to fit sampled data.

3.1 Seismic data

In 1988, Noteby AS conducted acoustic profiles over Eidangerfjord. Among the conclusions of the survey are two that are important to magnetic modeling. First, the angle of the bedrock slope on the east side of Eidangerfjord is significantly steeper than on the west side. Second, in Noteby report 44111-1 (Noteby, 1988) the carbonate-larvikite contact is placed 200m to 400m off the eastern shoreline of Eidangerfjord. Although the entire fjord was profiled E-W with a line spacing of 50m, only two E-W seismic profiles are presented in the report. I examined these two profiles carefully, and the point of the carbonate-larvikite contact I was in close agreement with the location on map 351 in the Noteby report. Although I was only able to check two seismic profiles, as is shown in this report, the location of the contact as derived from magnetic modeling is consistent with the contact as shown in the Noteby report.

3.2 Rock magnetic properties

For a given set of magnetic data, an infinite number of models can be found that fit the data, and many of these may be geologically and geophysically reasonable. In order to reduce the number of possible reasonable solutions to choose from, rock samples were taken from each of the major units and rock properties, including magnetic susceptibility and remanence, were measured on each sample. Andreas O. Harstad of Norcem AS chose the sites and formations to be sampled. In all, 135 samples were collected and measured. Details of these samples are shown in the Appexdix to this report. Generally speaking, the sandstone, slate, and carbonate samples were non-magnetic, having susceptibilities in the range from 0.0001 to 0.001 SI (System Internationale). Granites and gneisses had susceptibilities from 0.0006 to 0.007 SI. Most of the larvikite and lardalite specimens have susceptibilities near 0.02 SI. Most amphibolite samples are near 0.001 SI, although one is as high as 0.02 SI. The most magnetic specimens were basalt or diabase samples. These have susceptibilities up to 0.1 SI, and are typically near 0.02 SI. Fig. 3 shows the magnetic susceptibility data from the samples superimposed on a magnetic anomaly map of Eidangerfjord.

Magnetic remanence was one of the properties measured on the samples. In some instances, remanent magnetism can dominate the susceptibility controlled (induced) component and

affect the magnitude and shape of magnetic anomalies. The ratio of remanent magnetism to induced magnetism is called the Koenigsberger ratio, or commonly, the Q-value. A Q-value greater than 1 implies dominant remanent magnetism. A Q smaller than 1 implies dominant susceptibility controlled magnetization. Q-values for the 135 samples are shown in the Appendix. The largest Q-values occur in sedimentary samples having very small susceptibilities. In such cases, a large Q is inconsequential because the magnetic anomaly produced is small irrespective of the dominant magnetic mode. The granite and gneiss samples generally have Q-values less than 1. Most of the larvikite/lardalite samples have Q-values between 0.1 and 1. This implies that magnetic induction is probably the dominant mode of magnetism, and that remanence can be neglected in modeling the Eidangerfjord magnetic anomalies, an exception being the larvikite body in L301 which required a remanent magnetization. Also, basalt samples near the top of Eidangerfjord, and in line with the central fjord anomaly had Q-values of about 2, so in the forward modeling section (3.5) I have considered both possibilities. A Q-value map is shown in Fig. 4.

3.3 Euler deconvolution

Euler deconvolution is an automatic method that uses spatial derivatives of the magnetic field for estimating the depth to the top of a magnetic structure (Reid et al., 1990). The user of the Euler algorithm controls only the structural index (denoted SI, not to be confused with the SI of magnetic susceptibility). The SI value describes the class of the magnetic structures under consideration. A structural index of zero applies to contact, whereas dikes and sills have a structural index of one. If the correct structural index is chosen, in the best cases reasonable depth solutions are generated and these line up along the boundary of the structure.

Shown in Fig. 5 are the Euler depth solutions for a contact model (SI = 0). South of 654500N, a contact is clearly outlined slightly to the east of the fjord's central magnetic high. Most of the depth solutions along the supposed fall in the range of 150-250m, and probably represent the contact between metasediments in the west and the larvikites in the east. Curiously, further north no contact solutions are generated. However, if a structural index of 1 is chosen (sills and dikes), a series of solutions are generated in the northern part of the fjord between the central high anomaly and the eastern shore (Fig. 6). Most of these depth solutions fall in the range of 100-200m.

Why should the Euler algorithm indicate a dike or sill instead of a contact in this area? The answer may lie in the geometry of the western wall of the larvikite intrusion. If the wall is not a smooth constant slope, but has a sharp abutment jutting out from it, as shown for example in Fig. 8-L101, then the Euler algorithm would identify such a structure as more like a sill than a contact. Thus, the sill solutions in Fig. 6 may mark the contact between the carbonates and a sill-like portion of the larvikite body jutting out from the main wall.

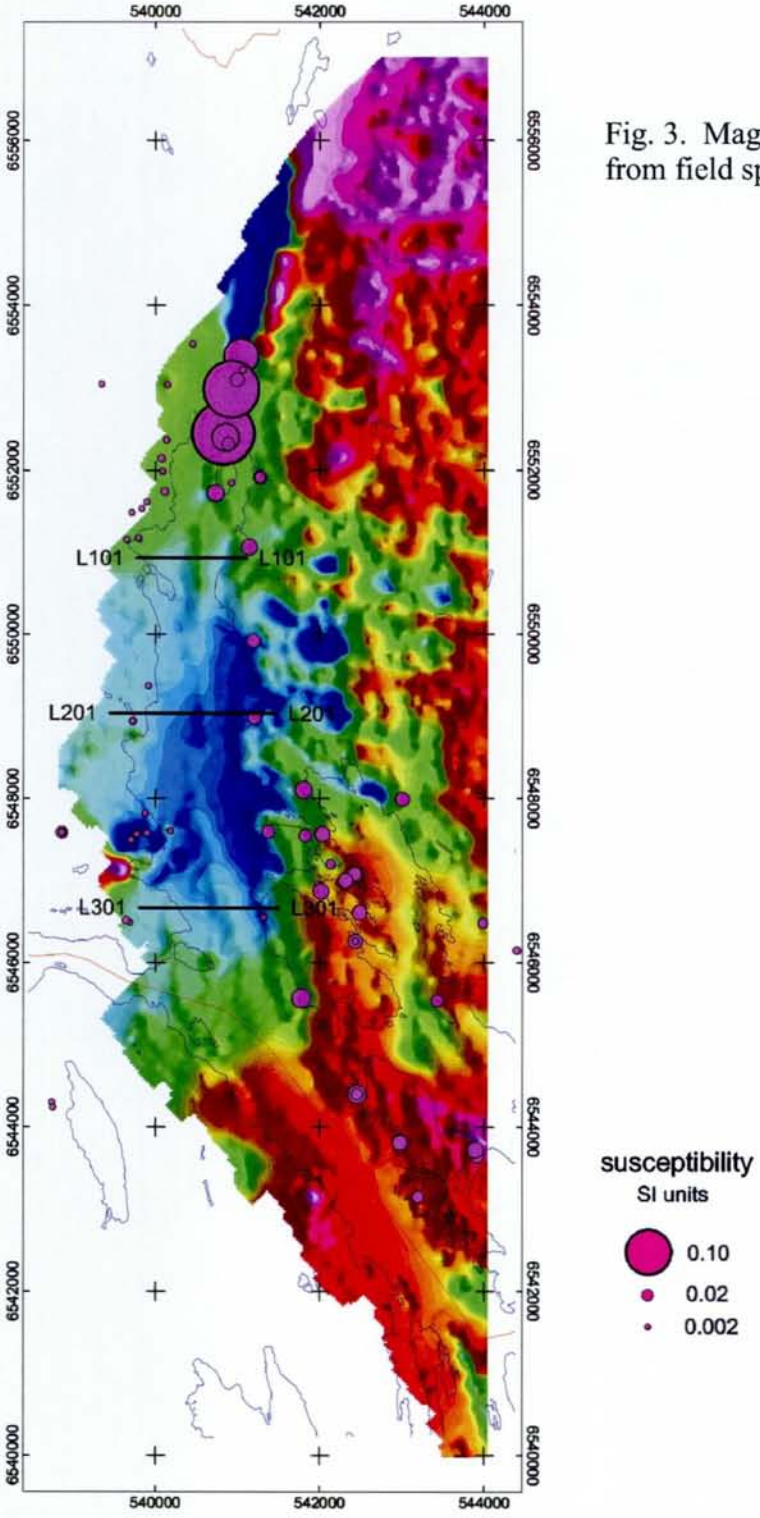

Fig. 3. Magnetic susceptibility as measured from field specimens.

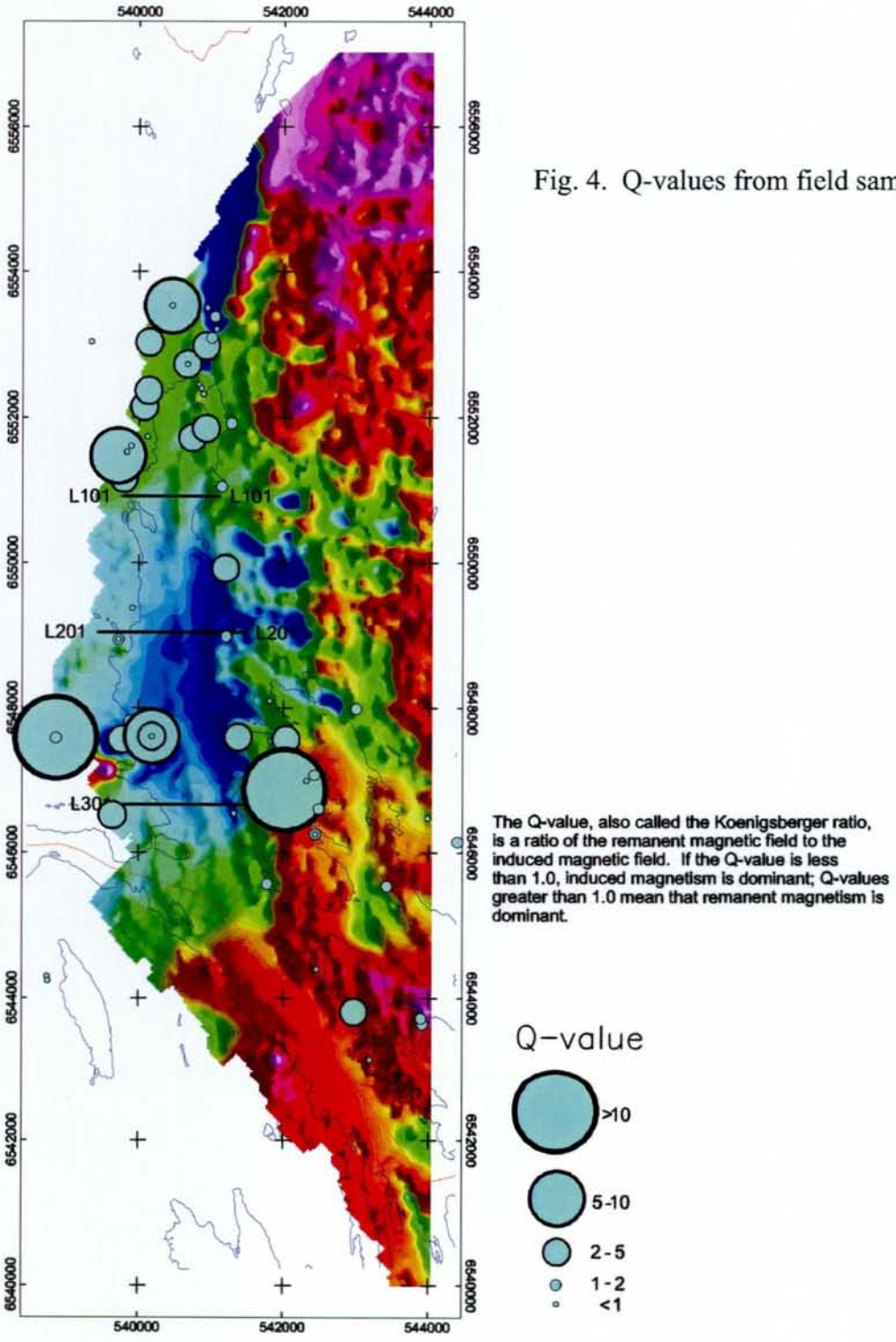

Fig. 4. Q-values from field samples.

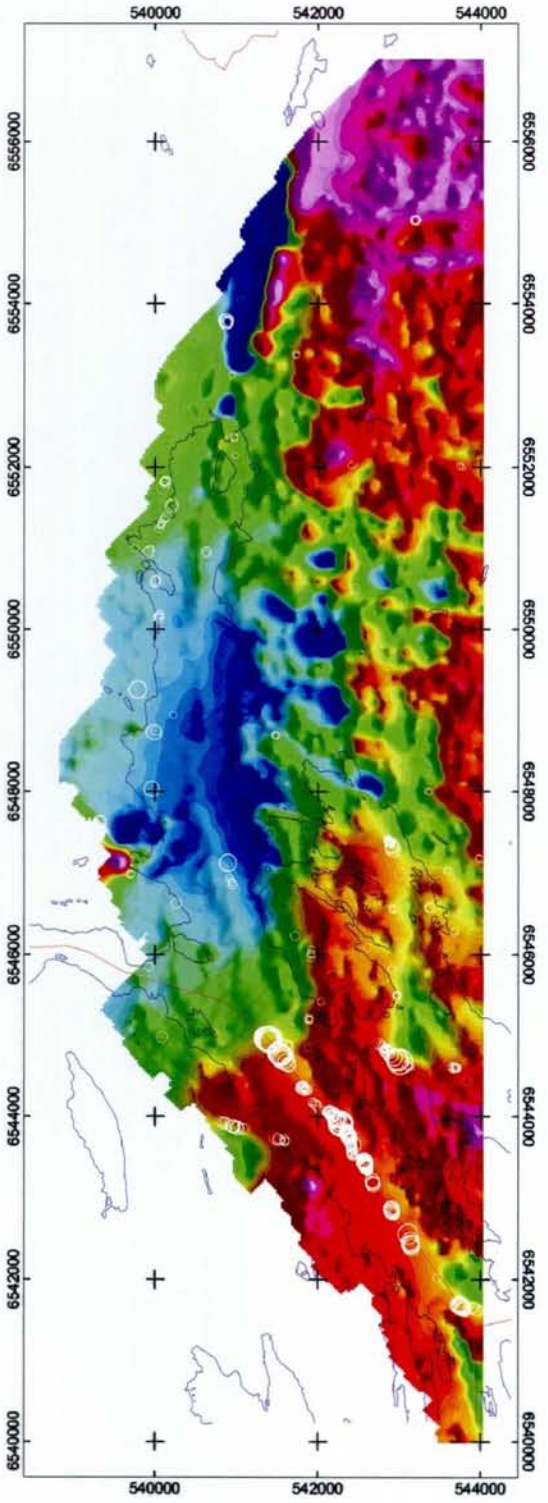

Fig. 5. Euler deconvolution of Eidangerfjord magnetic data using a structural index of 0. Depth to supposed contact is proportional to the size of the circle.

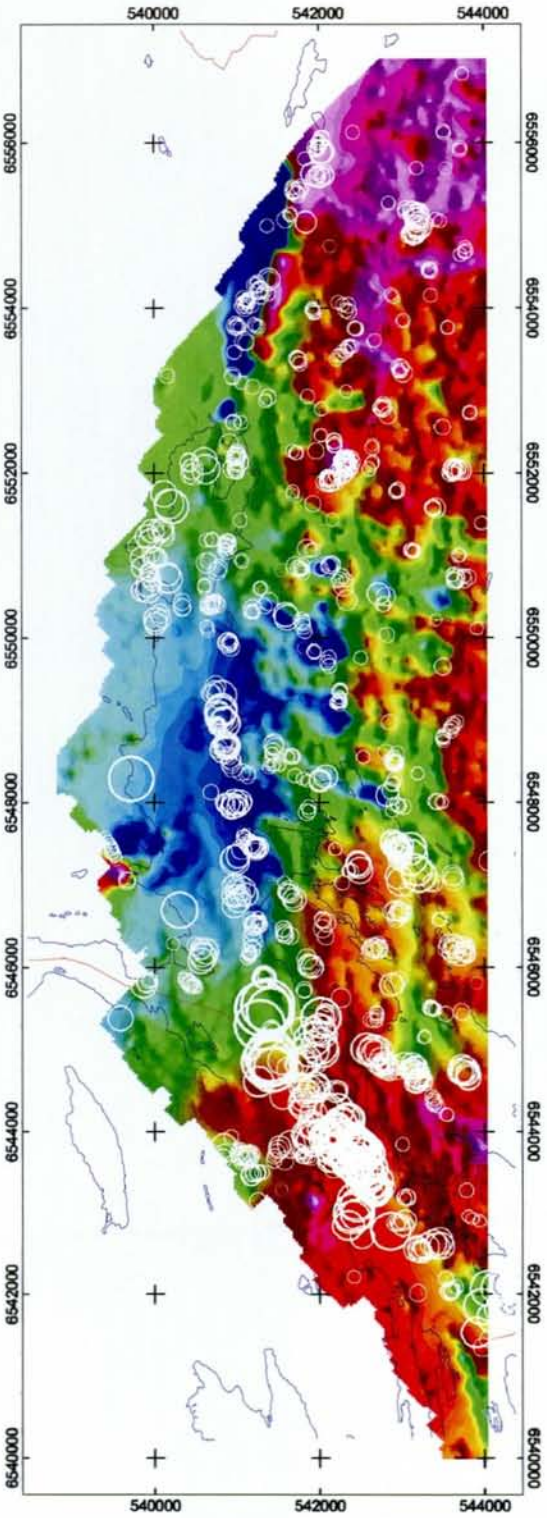

Fig. 6. Euler deconvolution of Eidangerfjord magnetic data using a structural index of 1. Depth to supposed dike or sill is proportional to the size of the circle.

3.4 Inversion for magnetic susceptibility

Before attempting forward modeling of the Eidangerfjord data, I used an inversion program to better estimate the magnetic susceptibilities of the bedrock. The inversion program divided the earth into long N-S striking rectangular prisms, each 50 m wide and with 1000 m vertical extent. The depth to the top of each prism was fixed at the estimated depth to bedrock across Eidangerfjord. The overlying sediments in the fjord are assumed non-magnetic. Using the Levenburg-Marquardt inversion algorithm (Marquardt, 1963), the magnetic susceptibilities of each prism were varied systematically until the computed field from the prisms gave a sufficiently close match to the measured data across Eidangerfjord.

Shown in Fig. 7 are the estimated magnetic susceptibilities of the prisms along each of three sampled lines denoted L101, L201, and L301 in Fig. 1. In each case, the computed data gave a good match to the measured magnetic data. All three inverse solutions have four general features in common. First, each line yields reasonable estimated susceptibilities for larvikite, mostly near 0.01 SI. These values are consistent with the measured susceptibilities of the field specimens. A second feature is that the magnetic susceptibilities drop to near zero just off the eastern coast of the fjord. This implies little or no magnetic material to depths of at least several hundred meters. The third feature common to all three sections is the section of very high estimated susceptibilities corresponding to the magnetic anomaly running through the center of the fjord. Each inversion shows a feature that is at least 200m wide having a magnetic susceptibility of 0.06 to 0.08 SI. This is an exceptionally high susceptibility and may correspond to a narrow magnetite-rich dike-like intrusion. However, as will be seen in the forward modeling section, the anomaly could also be cause by rock having a susceptibility consistent with magnetic rocks underlying the western side of the fjord. The fourth common feature is the moderately high estimated susceptibilities of the prisms near the western side of the fjord. The susceptibilities fall into the range of about 0.015-0.02 SI. Susceptibilities of field samples from rock units on the western side of the fjord show the carbonates to be nearly non-magnetic, having susceptibilities near zero. The Precambrian gneisses and granites have variable magnetic susceptibilities, but these generally fall below 0.002 SI. The high estimated susceptibilities from the inversion program require the presence of a moderately magnetic body beneath the carbonates on the western side of the fjord. The amphibolite/metagabbro unit exposed west from Eidangerfjord may be the source for this western magnetic body (not the central fjord body). If so, they would have to be more pervasively magnetic than the field samples indicate. Also, because the amphibolites are older than the carbonates, they would not explain the inferred heat source of Harstad (1999). A younger igneous intrusion seems an equally likely candidate for the western magnetic body.

Fig. 7. Results from inversion of magnetic data for magnetic susceptibility for sampled lines L101, L201, and L301. Top panel shows measured data (diamond symbols) and computed field (solid curve). Computed field is based on the susceptibility and depth model shown in the middle and bottom panels.

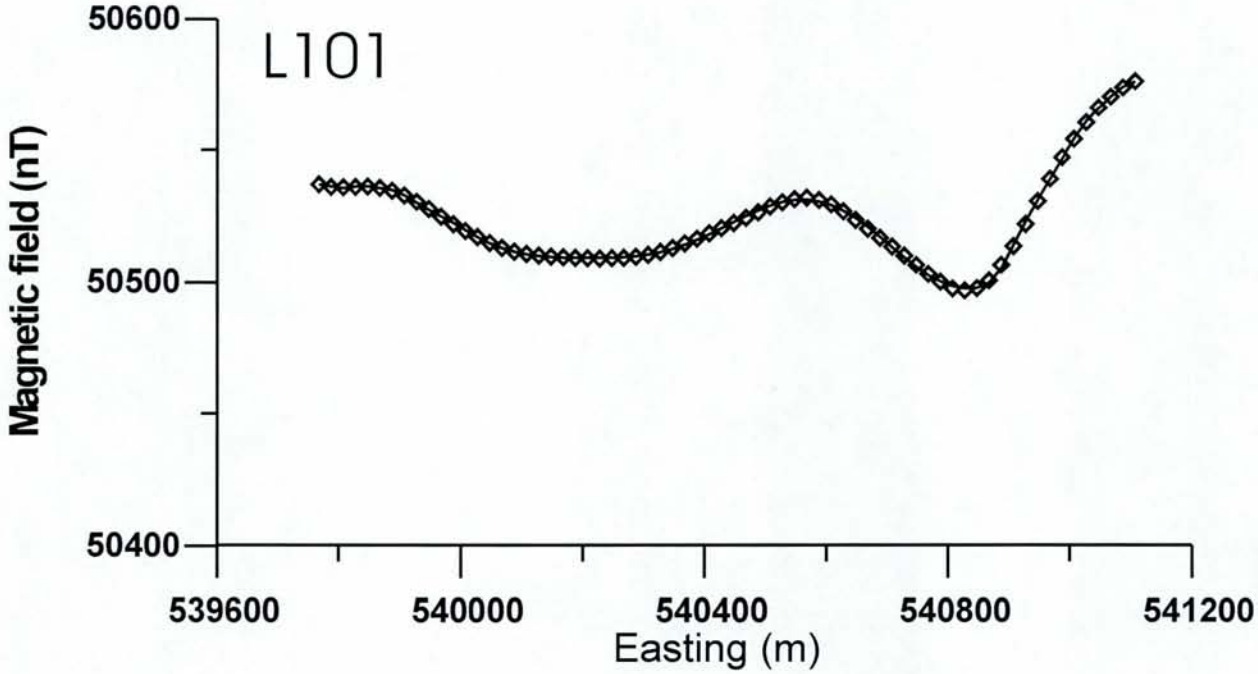
L101
Magnetic field (nT)
50600
50500
50400
539600
540000
540400
540800
541200
Easting (m)

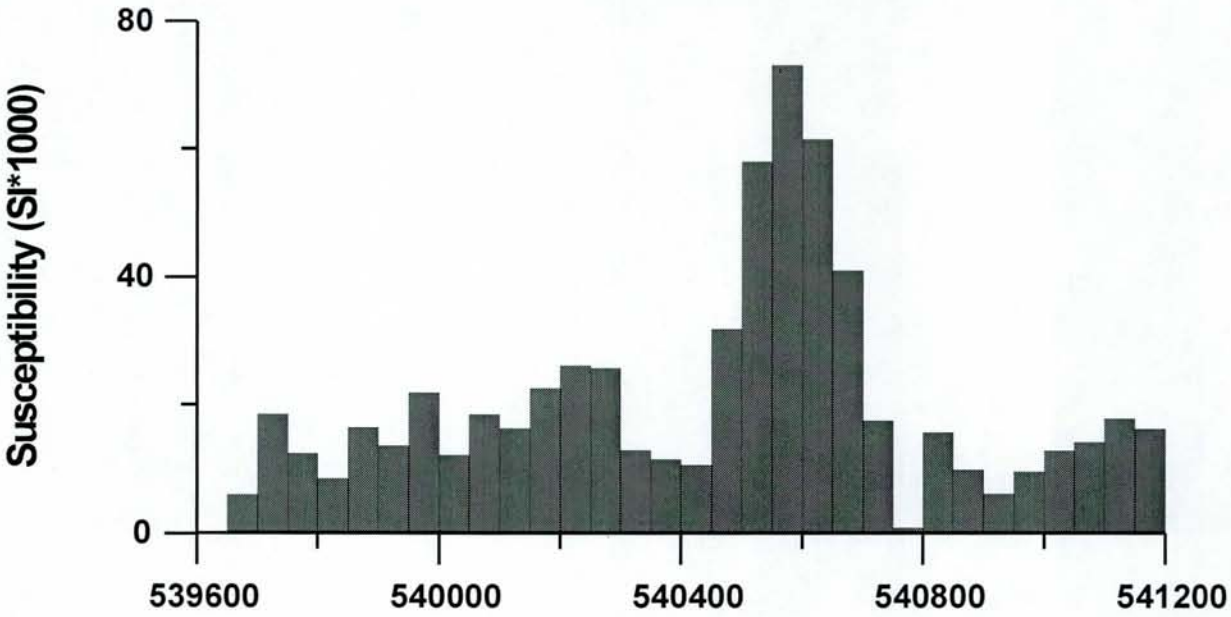
Susceptibility (SI*1000)
80
40
0
539600
540000
540400
540800
541200

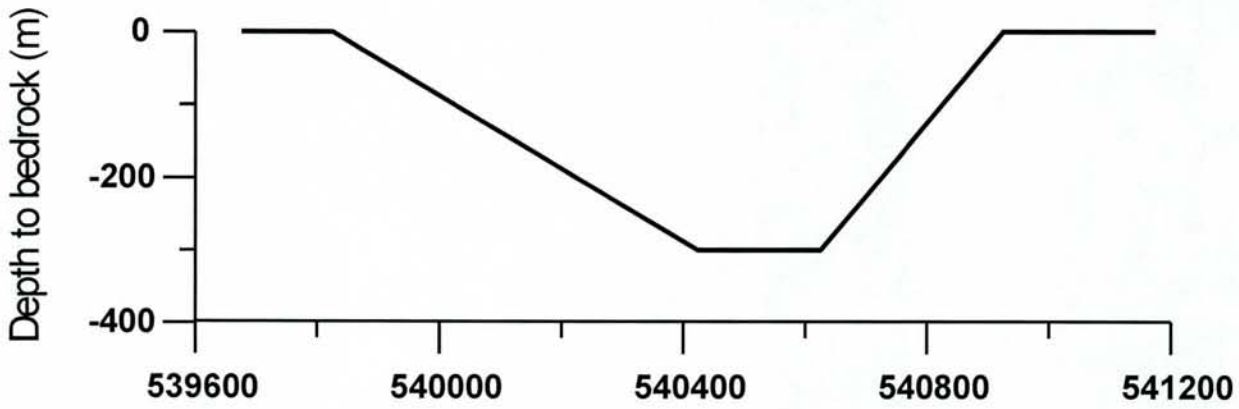
Depth to bedrock (m)
0
-200
-400
539600
540000
540400
540800
541200

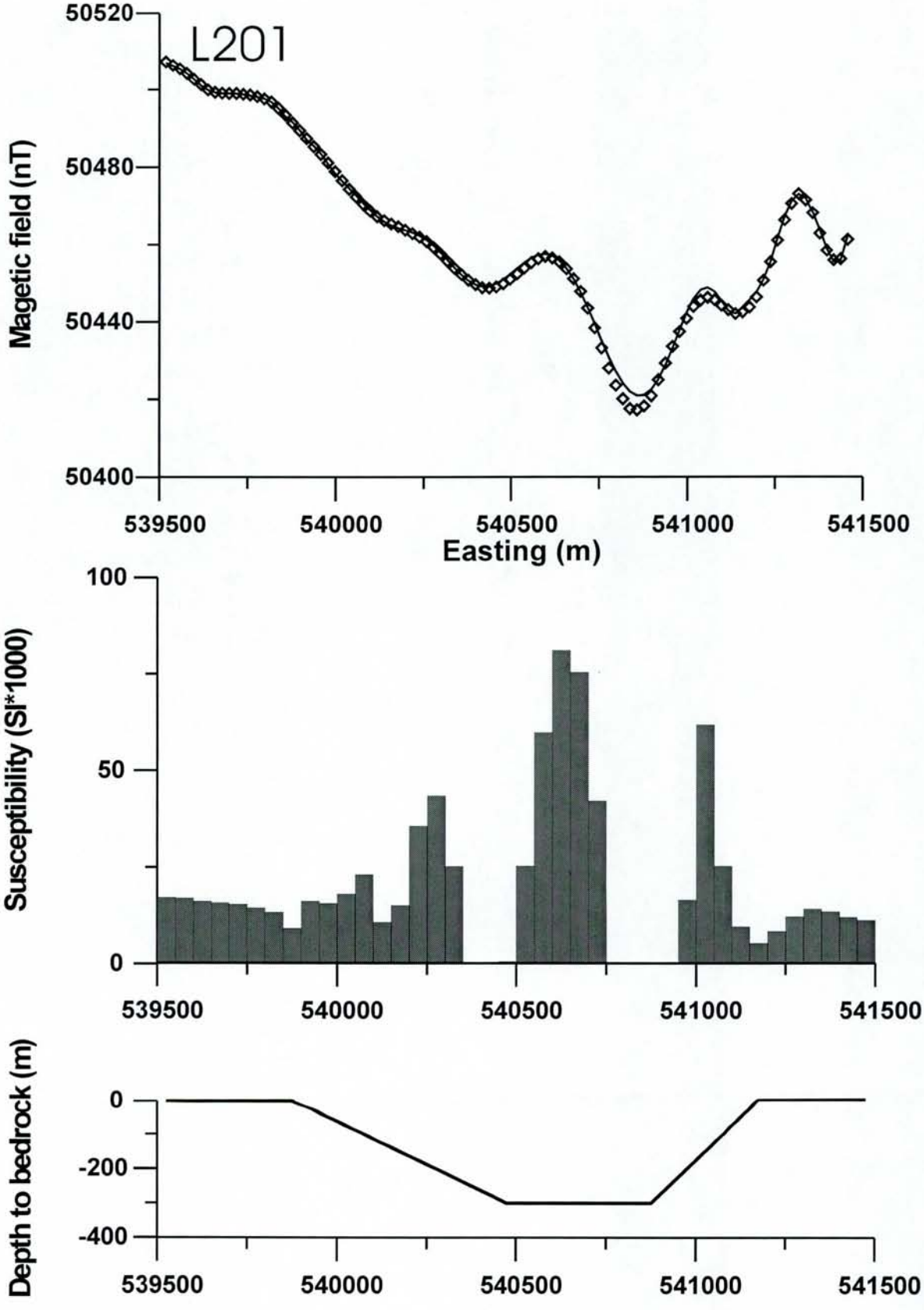
L201
Magetic field (nT)
50520
50480
50440
50400
539500
540000
540500
541000
541500
Easting (m)
Susceptibility (SI*1000)
100
50
0
539500
540000
540500
541000
541500
Depth to bedrock (m)
0
-200
-400
539500
540000
540500
541000
541500

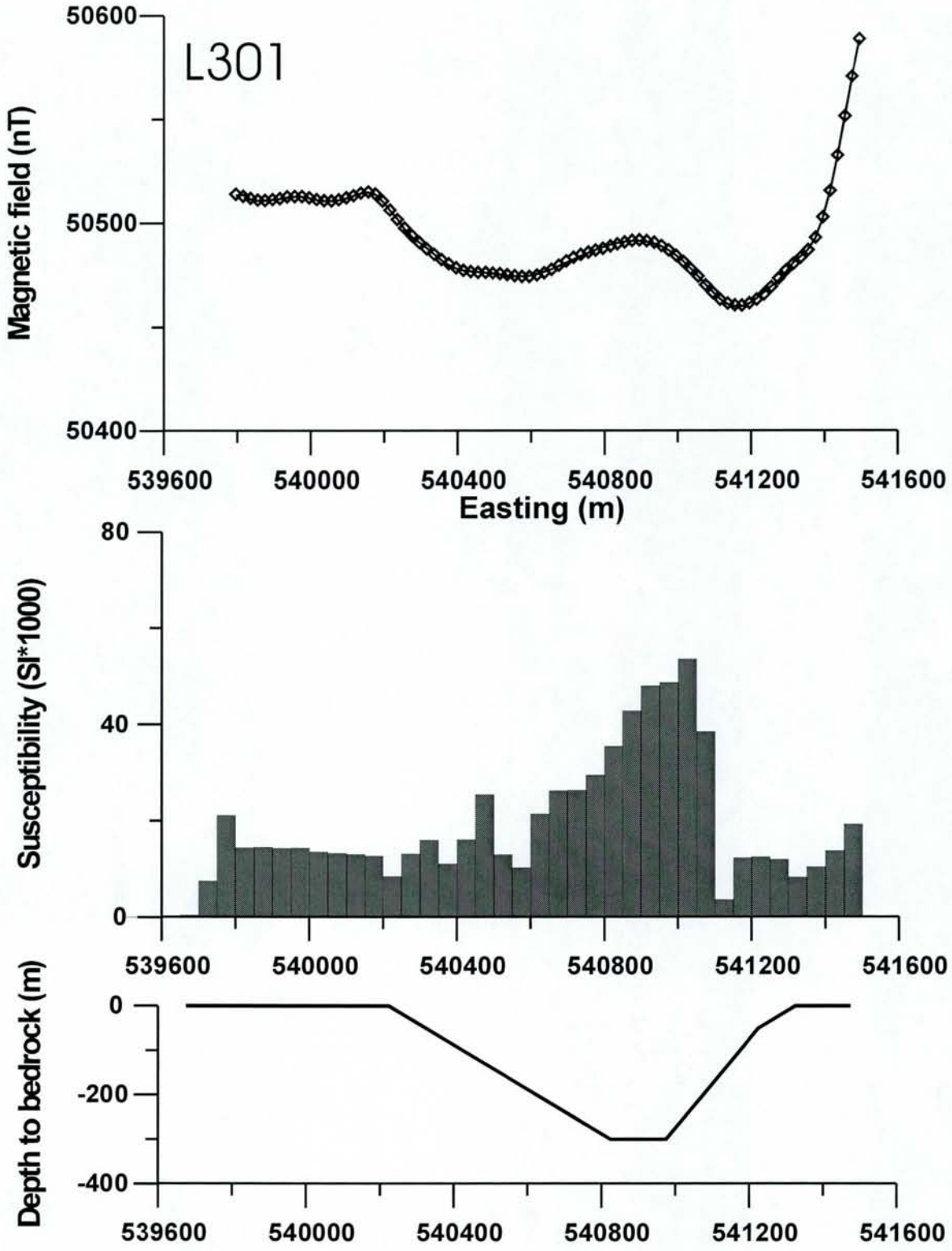
L301
Magnetic field (nT)
50600
50500
50400
539600
540000
540400
540800
541200
541600
Easting (m)
Susceptibility (SI*1000)
80
40
0
Depth to bedrock (m)
0
-200
-400

3.5 Combined forward and inverse modeling

Using the rock magnetic properties and the inversion results from the previous section, I was able to model the magnetic data using Encom's ModelVision software (Encom, 1999). ModelVision allows the user to combine forward and inverse modeling to achieve an accurate fit to a line of magnetic anomaly data. I initially tried modeling the magnetic data with one magnetic body, varying the shape of the body to fit the magnetic anomaly. However, when doing this I found that the thickness of a section of the model near the eastern side of the fjord had to be made zero. The presence of any magnetic material off the eastern coast of the fjord resulted in a poor fit to the data. Therefore, two magnetic bodies at minimum are necessary to obtain a close fit to the data. The models I show are the result of fitting the data with three bodies (Fig. 8) and two bodies (Fig. 9). For reasons I will later explain, I consider the three-body models in Fig. 8 to be the most likely solution.

Shown in Fig. 8 are models and data fits for each of the three lines shown in Fig. 1. In each case, at least three magnetic bodies were used to obtain the fits. L201 required four bodies to fit the data. In each model, the carbonate-larvikite contact is represented by the boundary of the larvikite body (the rightmost body in each model). These models are consistent with the contact as estimated by the Euler deconvolution method, and also with the contact based on the seismic data. Of interest is the shape of the larvikite wall. Its westernmost point is near the top, and it slopes inward to the east. This eastward slope begins to change in L301 to a westward slope, and judging from the Euler contact estimates in Fig. 5 south from L301, the sharp sill-like 'nose' that protrudes from the top of the may have disappeared in the south. L301 also requires that the larvikite body be assigned significant remanent magnetization, in keeping with the high Q-values measured from field samples collected in this area. In the model I used Q = 0.7 with the Permian paleopole, i.e. a remanent inclination of -40° and a remanent declination of 200°. Solutions without remanence resulted in the top of the larvikite body being placed too deep at the eastern shoreline.

With the three-body models, a narrow, highly magnetic body produces the central fjord anomaly. The magnetic susceptibility required is about 0.09 SI. This is an exceptionally high susceptibility, but a basalt sample taken from the exposed contact at the north end of Eidangerfjord measured 0.12 SI, so the modeled value is not unreasonable. The central magnetic body in each of the three lines has a significantly different shape, but is about 75-200m wide. In L301, the line nearest the Norcem mine, the top of the body terminates at a depth of 250 m, and so may intersect the carbonates. If so, this would no doubt impact mining operations.

For each line modeled, I found that a western magnetic body, probably separate from the central body, was required under the western shore of Eidangerfjord to explain the rise in the measured magnetic field from east to west approaching the western shore. Inversion

Fig. 8. Results from combined forward modeling and inversion of magnetic data for sampled lines L101, L201, and L301. Three major magnetic bodies were assumed. Shape and magnetic susceptibility (SI units) of the magnetic bodies are shown. Depth is in meters below surface. The '+' symbols represent measured data, and solid lines are computed from the model. L201 required a fourth body beneath the larvikite intrusion in order to fit the data. L301 required that the larvikite body have remanent magnetization.

L 101

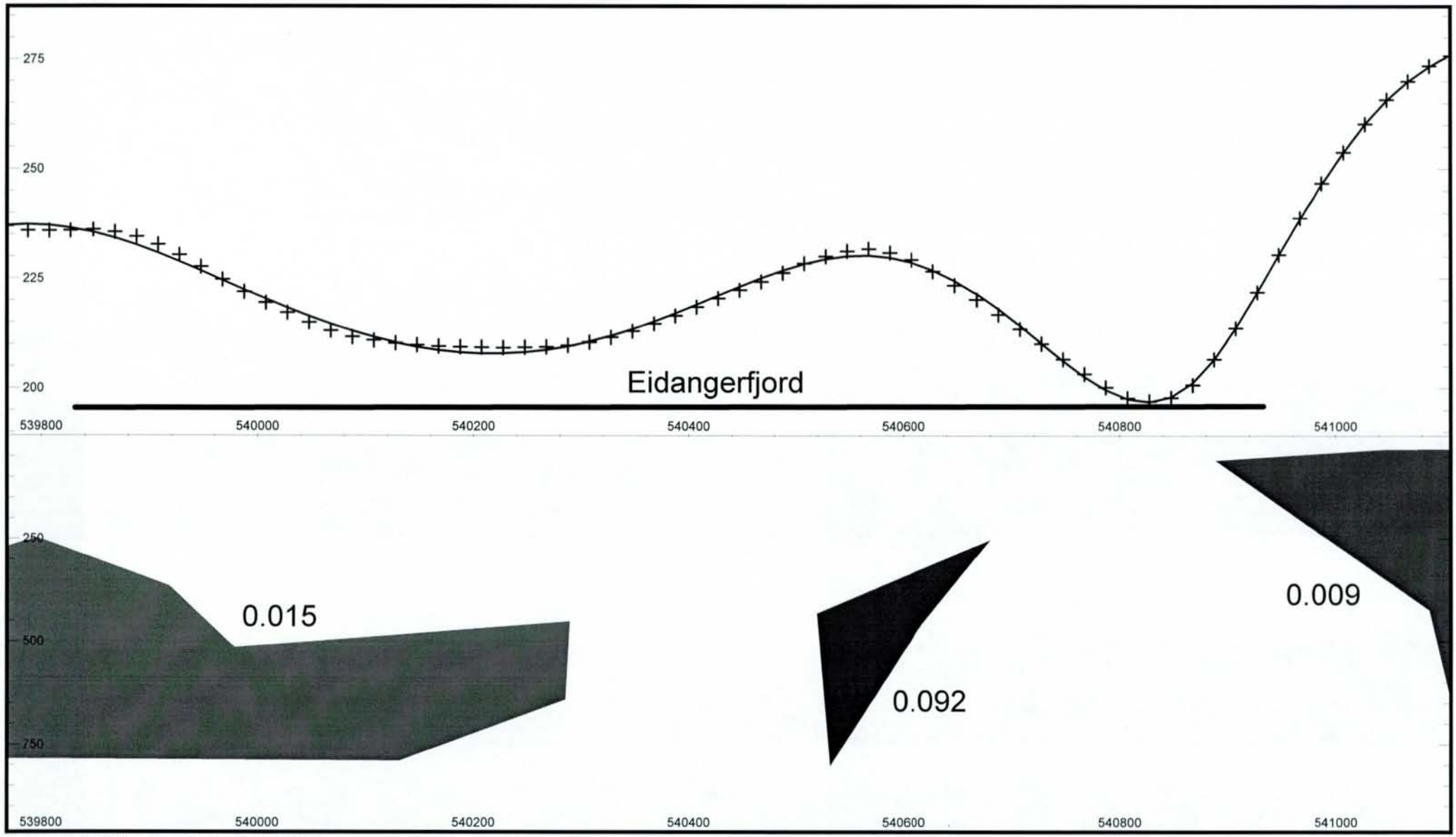

Norway GS ModelVision Pro - Thu Jun 22 10:42:23 2000

L 201

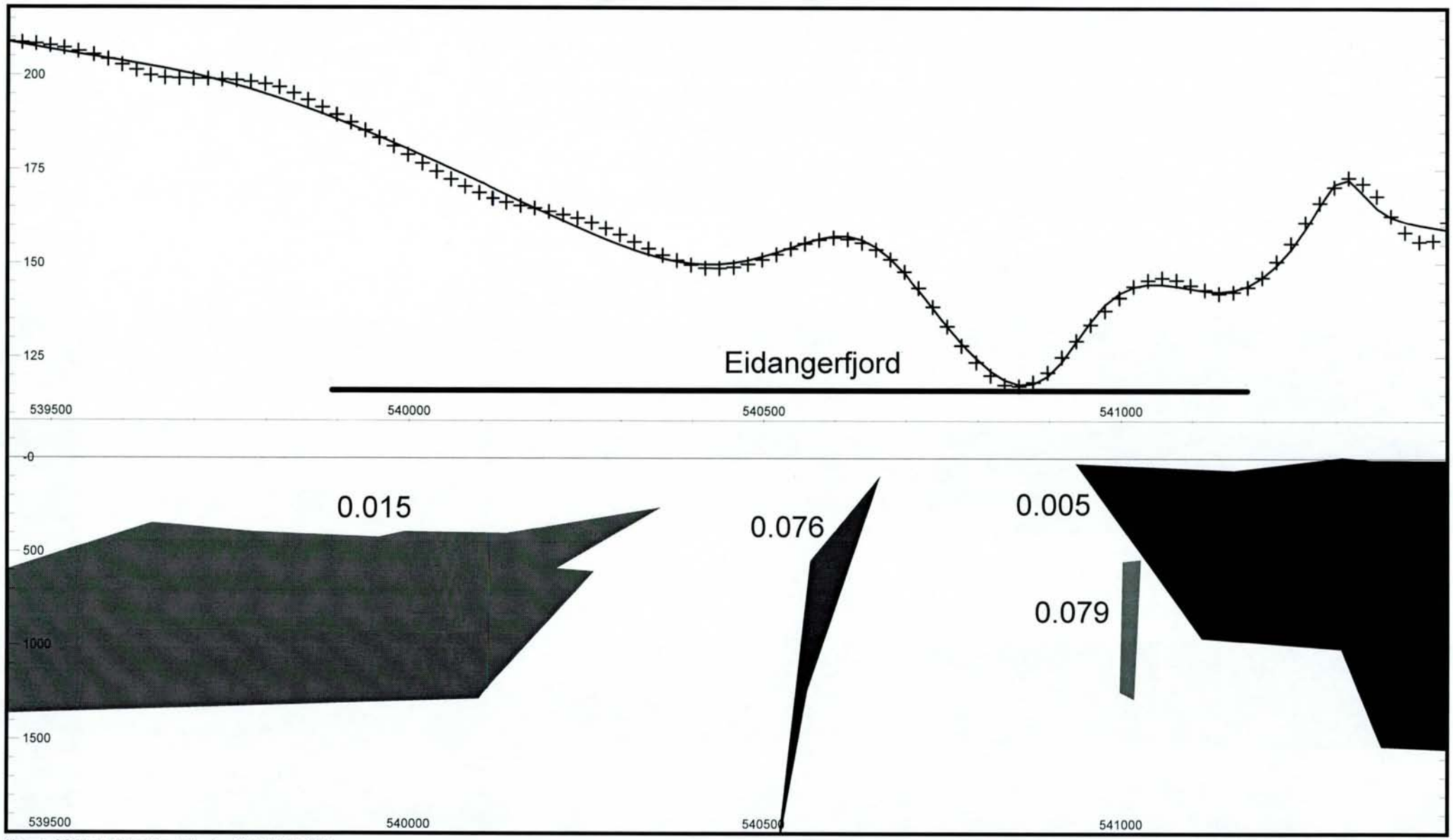

Norway GS ModelVision Pro - Thu Jun 22 11:04:12 2000

L 301

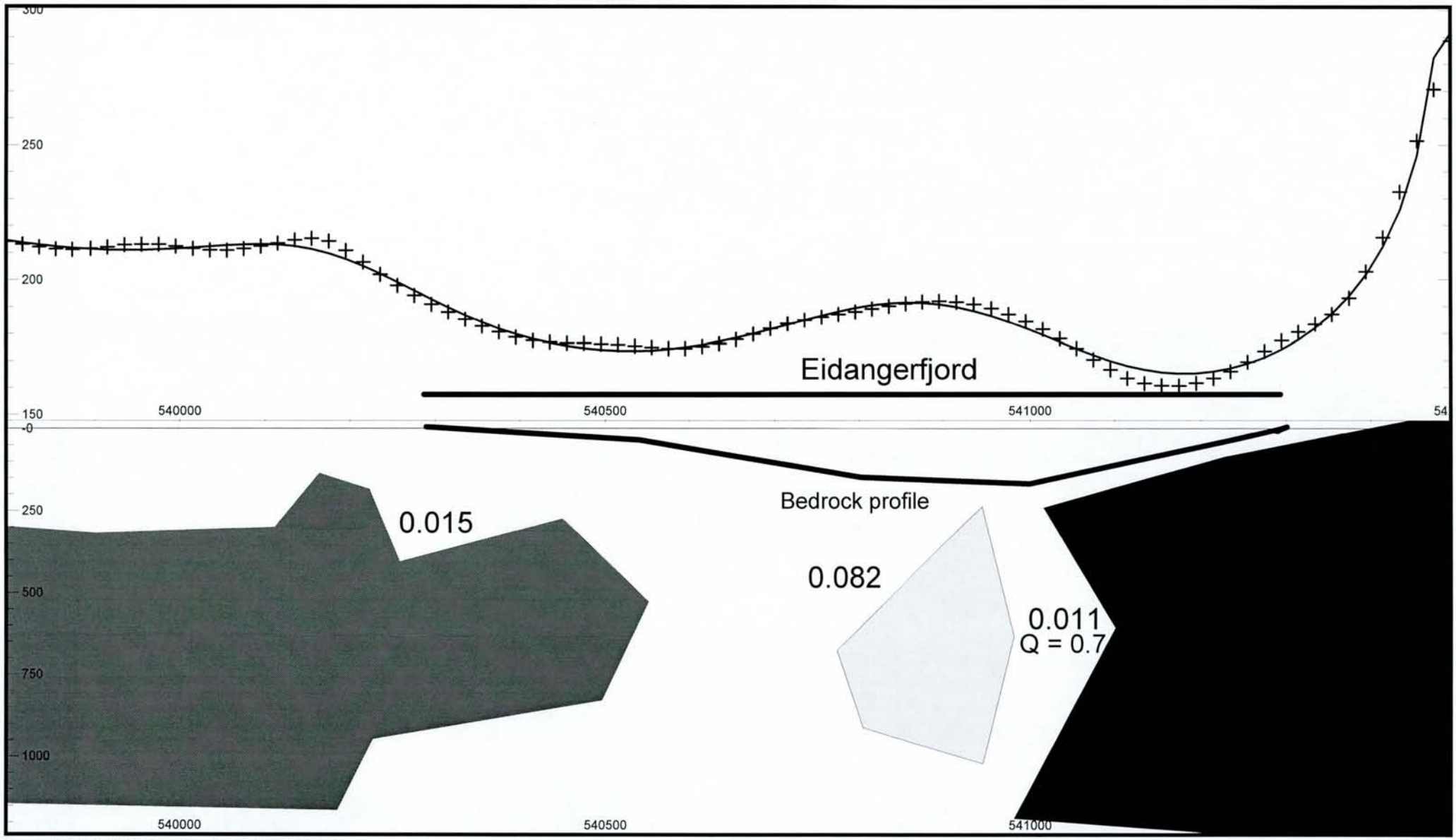

Norway GS ModelVision Pro - Mon Jun 26 14:02:01 2000

estimates for this body yielded susceptibilities near 0.015 SI. This susceptibility was used for the western body in the forward models, and did not change during the final inversion steps. Modeling results indicate the body has an irregular surface and extends eastward at least 200-300m under the fjord. The depth to the top of the body at the edge of the fjord at the location of L301 is about 400m.

I also examined the role of magnetic remanence in producing the anomalies. Some basalt samples at the top of Eidangerfjord have Q-values of about 2, i.e. remanence dominates induction by a factor of 2. If we presume remanence is due to the Permian paleofield, then the remanent inclination is about -40° and the remanent declination about 200°. Using these values I tried to adjust the shape, depth and susceptibility of the center body in order to match the data. Fig. 9 shows the three-body solution for L101, L102, and L103. Only the central body was assigned a remanent field (Q=2). In L101, the field data can be matched only if the western body extends well into the fjord, almost abutting the remanent body. L102 is little changed from the non-remanent case. It is almost impossible to match the L103 data with a remanent central body. The central body has to be made almost vanishingly thin and the western magnetic unit has to be extended almost to the opposite side of the fjord.

The previous models used at least three separate magnetic bodies to model the data. However, it is possible to achieve equally good fits to the data with only two bodies. If the magnetic body on the western side of the fjord extends further into the fjord and thickens at the eastern end, the mid-fjord anomaly can still be modeled. Fig. 10 shows models for each of the three lines based on the assumption of two bodies. Because of the lower magnetic susceptibility, the portion of the body creating the central fjord anomaly must be larger and a little shallower than in the three body models. This shallower body would probably extend into the carbonate unit and severely impede mining operations.

4 DISCUSSION AND CONCLUSIONS

While bearing in mind the non-uniqueness of magnetic modeling solutions, this modeling exercise shows three major magnetic bodies, probably separate igneous intrusions, beneath Eidangerfjord. Of these three, the larvikite complex on the eastern side of the fjord is the only exposed body. The other two are inferred from magnetic models. One of the inferred bodies appears to be an irregularly shaped sill-like body under the western side of Eidangerfjord. The depth to the top of this body is variable, but beneath the fjord it may be 400-500m below the surface of the fjord. Its magnetic susceptibility—about 0.015 SI—is typical of gabbro and is substantially higher than that of the larvikite (0.005-0.009 SI), so the rocks making up the body may be compositionally different from the larvikite as well. There is no good way to estimate the thickness of the igneous body from the magnetic data, but models that use a

Fig. 9. Results from combined forward modeling and inversion of magnetic data for sampled line L101, L102, and L103. Three major magnetic bodies were assumed, and the central body is assigned a high remanent magnetization. Shape and magnetic susceptibility (SI units) of the magnetic bodies are shown. Depth is in meters below surface. The '+' symbols represent measured data, and solid lines are computed from the model.

L 101--High Q central body

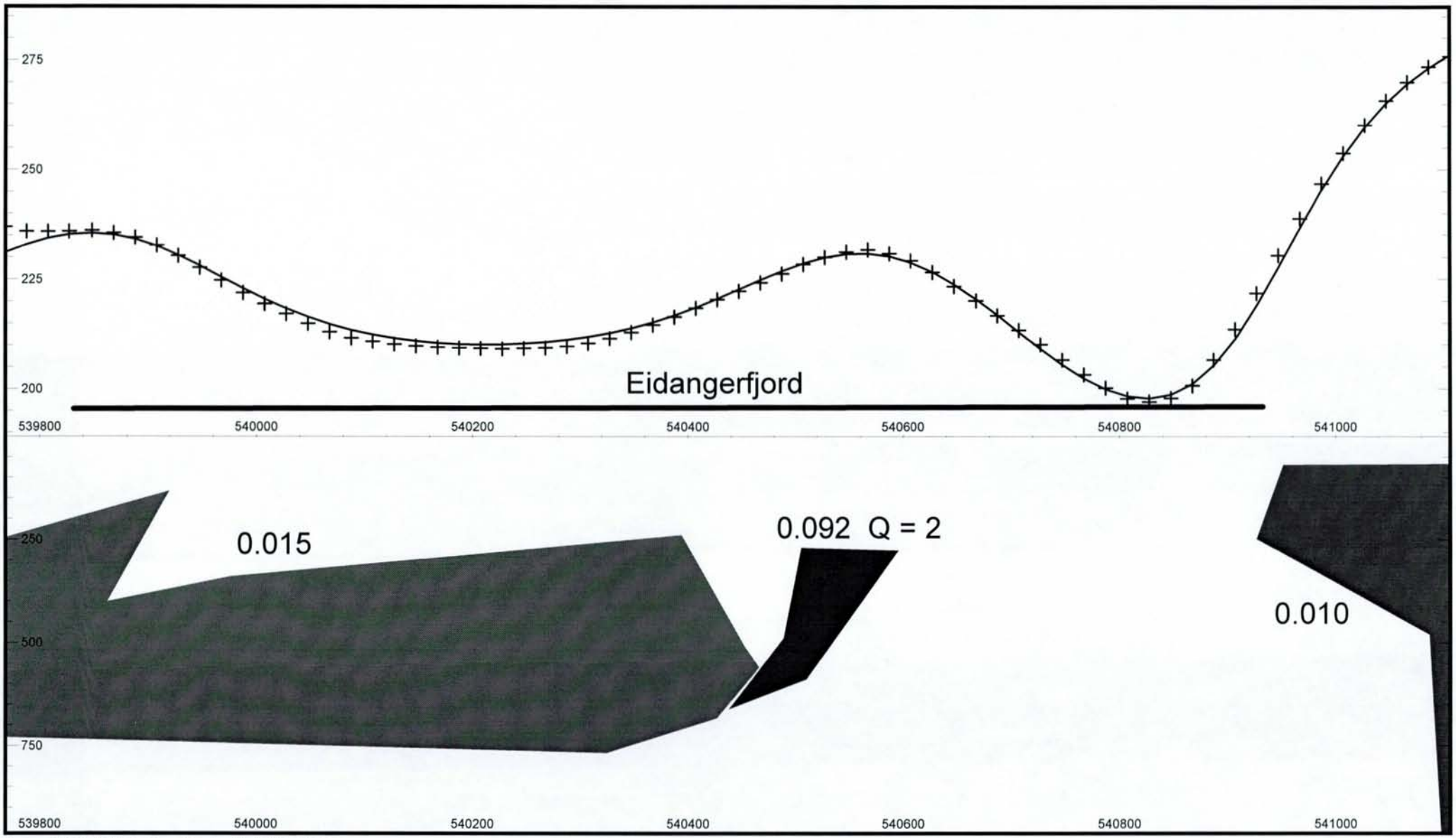

Norway GS ModelVision Pro - Thu Jun 22 10:42:23 2000

L 201 - High Q central body

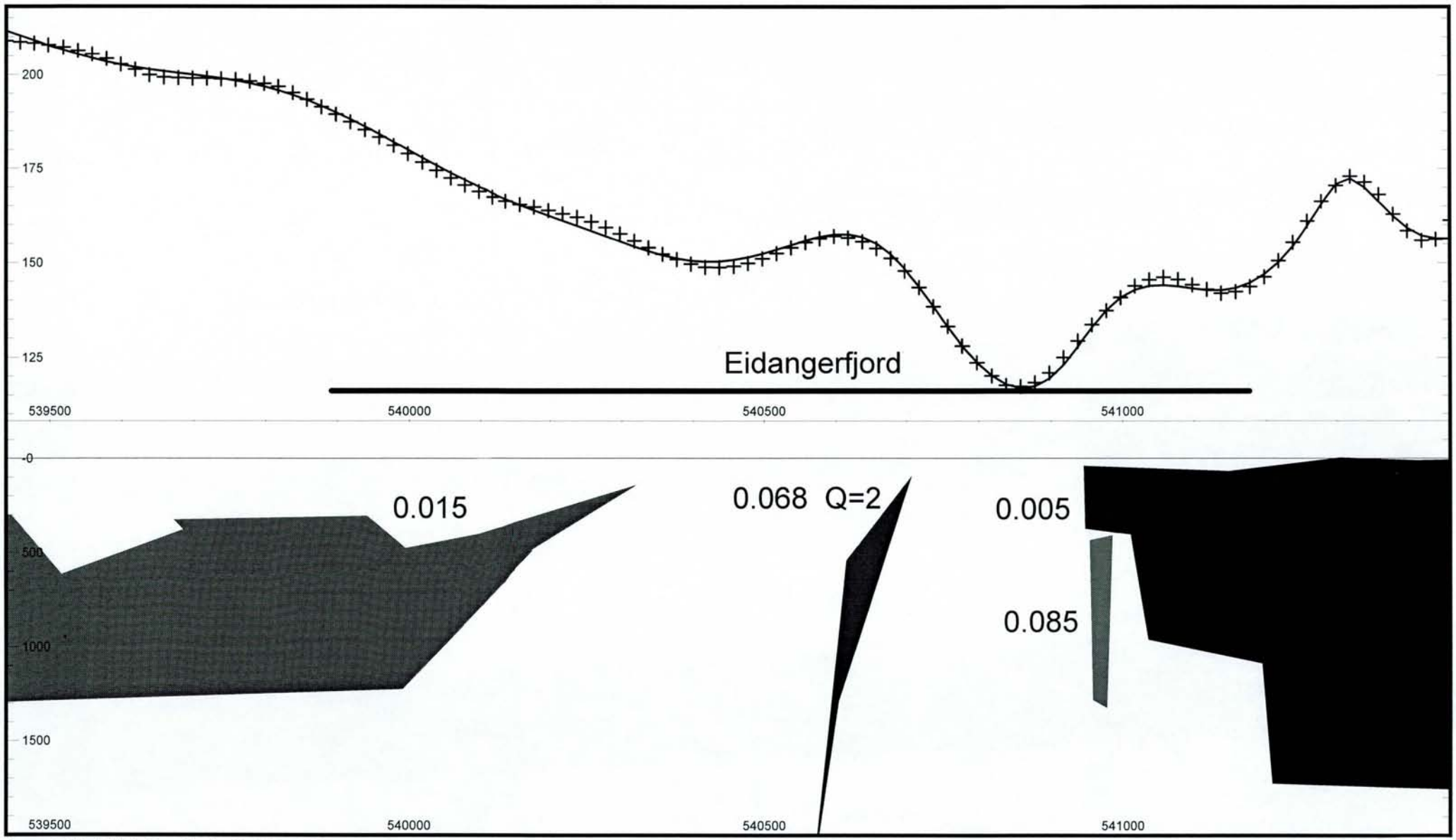

Norway GS ModelVision Pro - Thu Jun 22 11:04:12 2000

L 301 - High Q central body

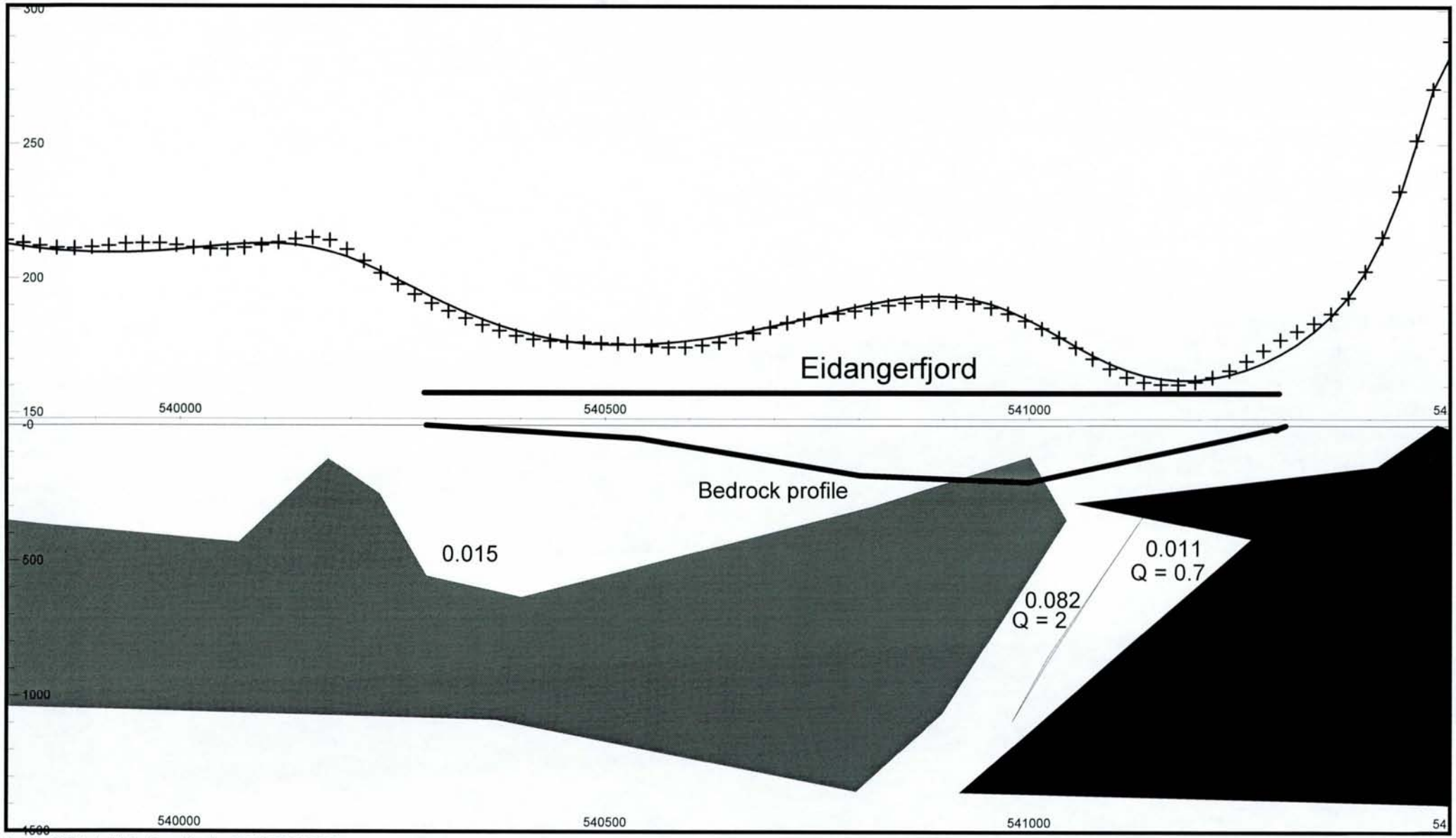

Norway GS ModelVision Pro - Mon Jun 26 14:02:01 2000

Fig. 10. Results from combined forward modeling and inversion of magnetic data for sampled lines L101, L201, and L301. Two major magnetic bodies were assumed. Shape and magnetic susceptibility (SI units) of the magnetic bodies are shown. Depth is in meters below surface. The '+' symbols represent measured data, and solid lines are computed from the model. L201 required a third body beneath the larvikite intrusion in order to fit the data.

L 101-v2

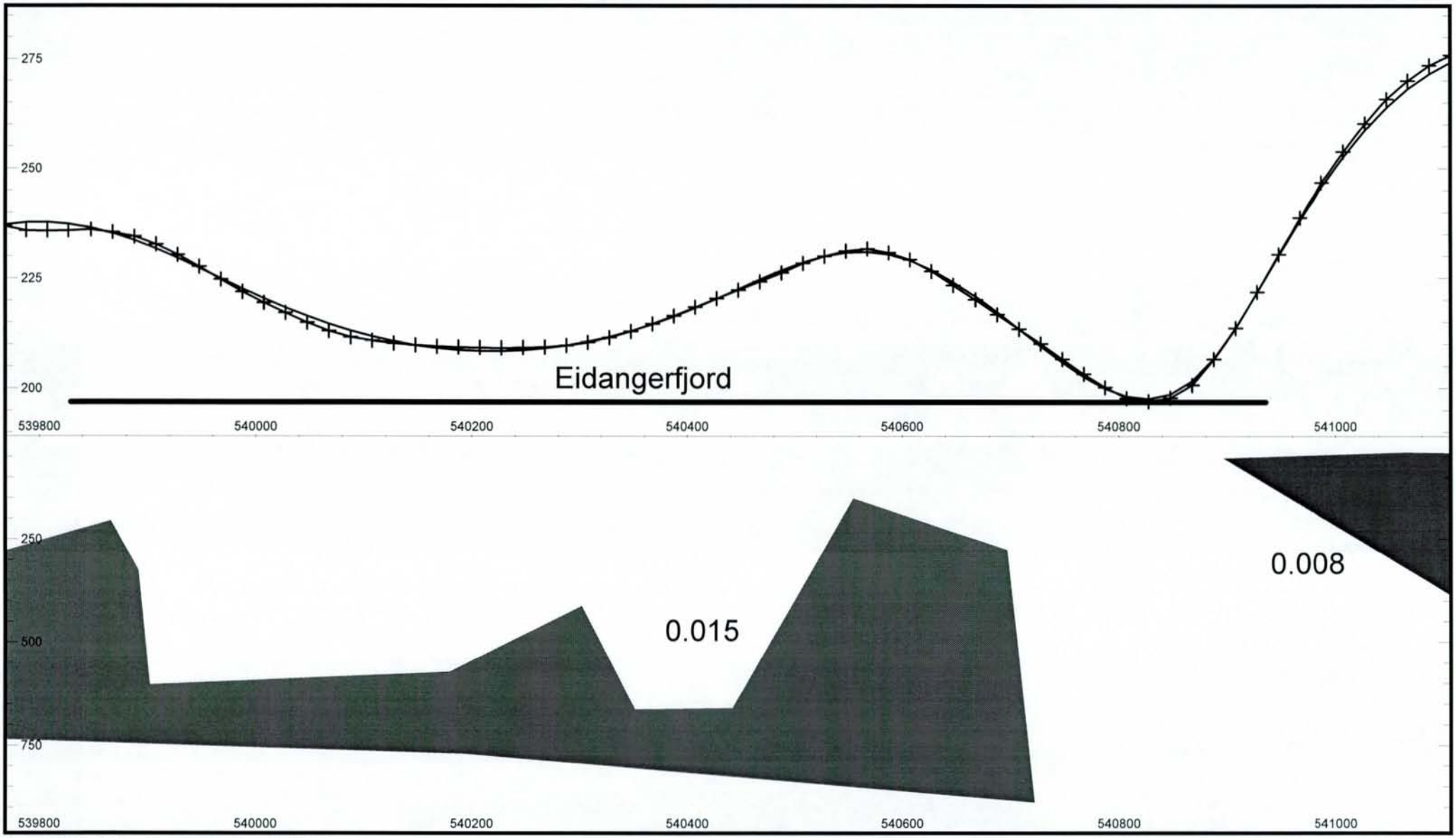

Norway GS ModelVision Pro - Sun Jun 25 13:38:44 2000

L 201 - v2

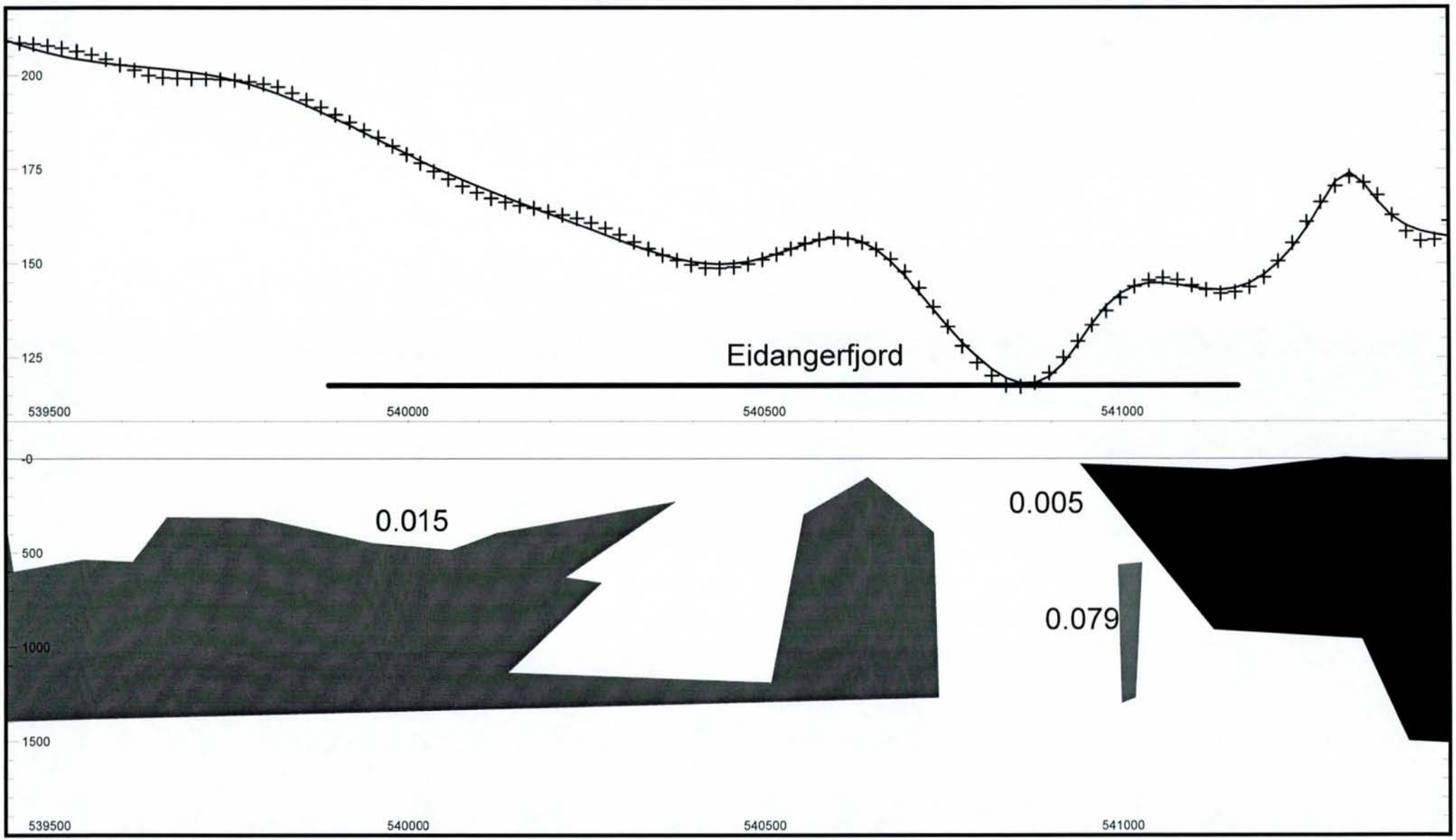

Norway GS ModelVision Pro - Sun Jun 25 13:54:46 2000

L 301 - v2

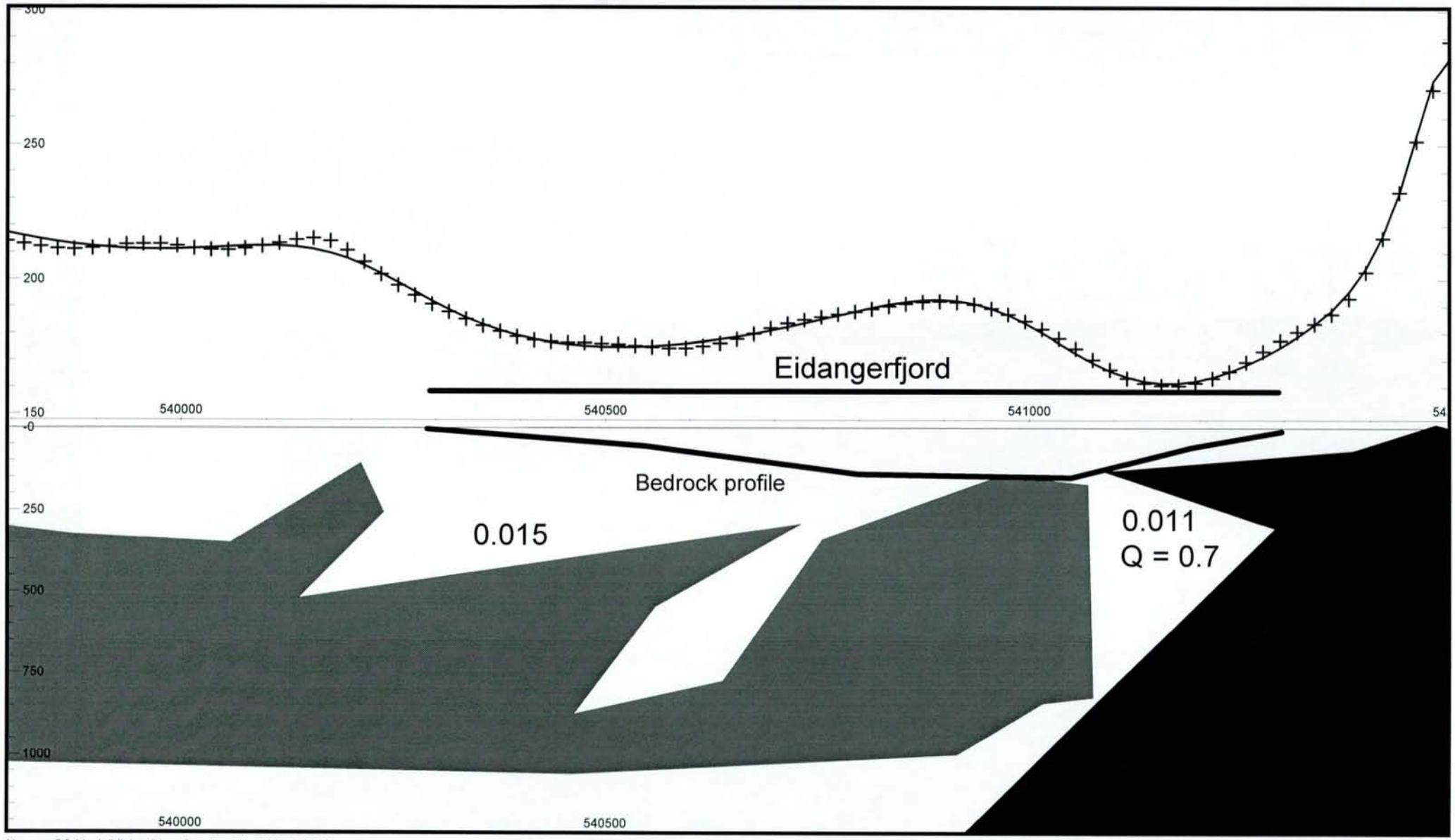

Norway GS ModelVision Pro - Sun Jun 25 14:08:42 2000

magnetic susceptibility of near 0.015 show the layer to be 200-500 m thick. It seems to be somewhat thinner beneath the fjord than further to the west.

Prior to the publication of the NGU magnetic data, Harstad (1999) inferred the presence of such a body based on his studies of contact metamorphism in the Porsgrunn-Eidanger aureole. He found that temperatures derived from numerical models were too low to explain the phase petrological temperature gradient and the observed calcite coarsening if the heat source was the larvikite body. A more nearby heat source was required to explain the observations. The magnetic data support this inference, so long as the western body is younger than the carbonates.

The second inferred igneous body causes the anomalous north-south trending magnetic high in the center of Eidangerfjord and is probably a series of dike-like intrusions intruded through fractures. Although it may consist of multiple intrusions, for simplicity I have modeled it as a single body. Its modeled magnetic susceptibility (0.07-0.09 SI) is an order of magnitude higher than either the larvikites on the eastern side of the fjord or the inferred igneous body on the western side (0.015 SI). If the estimated magnetic susceptibility is correct, the intrusion is at least 200 m thick laterally, and may be thicker. Still higher susceptibilities would imply a thinner body, but significantly higher susceptibilities than 0.1 SI are not common in igneous rocks. Each of the three cross-sections shows the body to be within 250 m of the surface of the fjord. If correct, the intrusion probably cuts into the carbonate unit and would therefore hinder to mining operations. As shown in Fig. 10, the central fjord anomaly can be reproduced using susceptibilities matching the western magnetic body. However, if the body producing the anomaly is an extension of the western body, the geometry requires that the body becomes thin on the western side of the fjord, then thickens again near the center of the fjord.

In my opinion, the three-body model of Fig. 8 is more probable than either the two-body model of Fig. 10 or the remanence model of Fig. 9. The susceptibilities of basalt samples near the top of the fjord are in the same high range as the modeled central fjord body. Furthermore, the central fjord anomaly is fairly regular and straight, whereas the western magnetic body is irregular. Presumably the eastern extension would also be irregular and would be unlikely to produce the straight central fjord anomaly. The remanence model is very different from line to line, and is therefore inconsistent with a geologically uniform and continuous structure.

Fig. 11 shows a very general schematic of what I believe to be the most probable model. The central fjord 'dike' may well be part of the Permian basaltic body north of Eidangerfjord, but is distinctly separate from the larvikites. If these two bodies are connected, it is at a depth unresolvable from either existing seismic or magnetic data.

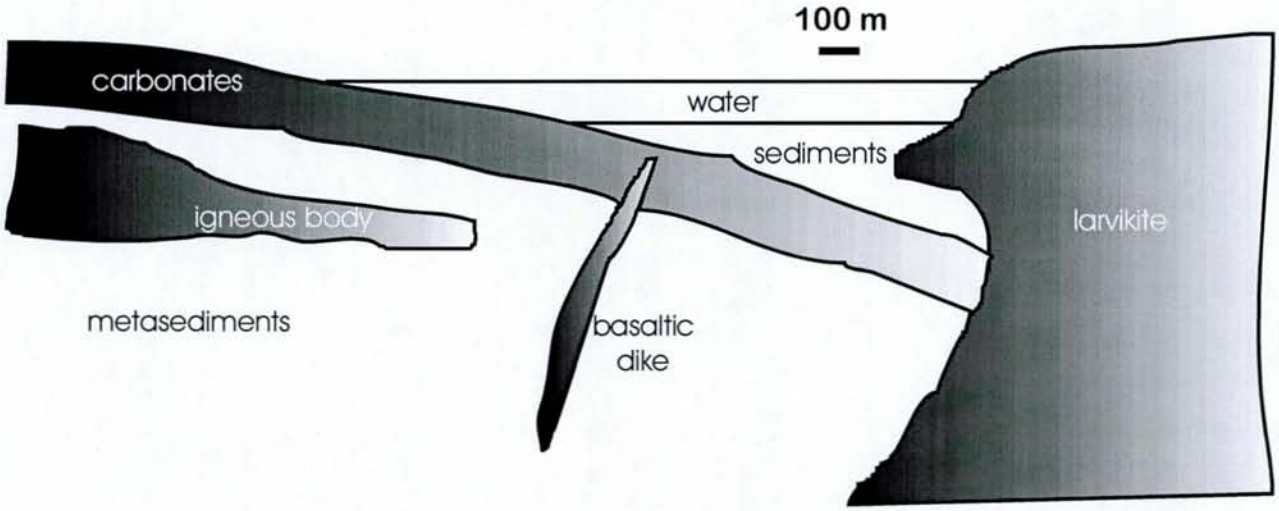

Fig. 11. Schematic drawing of geological structures beneath Eidangerfjord

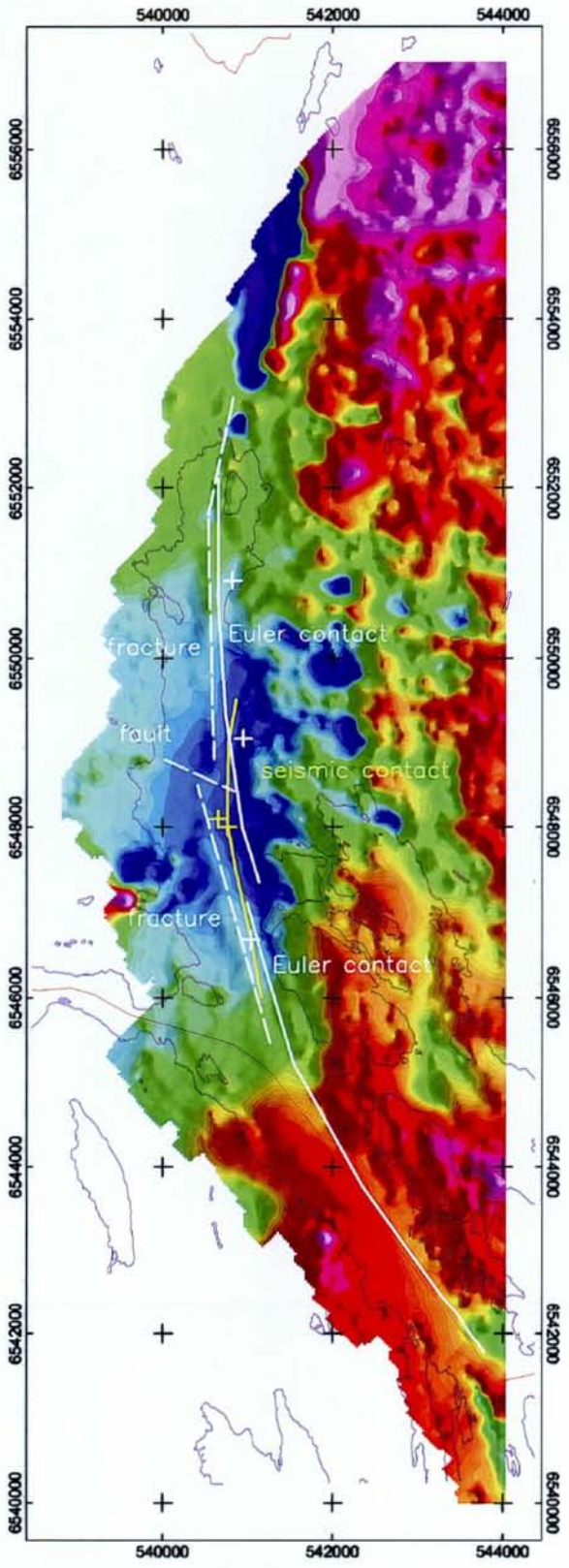

Fig. 12. Solid curves represent estimated location of larvakite-carbonate contact in Eidangerfjord. White curve is based on Euler deconvolution. Yellow curve is from Noteby seismic data. Dashed lines represent possible fractures along which the proposed central fjord dike was intruded. Yellow '+' symbols represent contact locations as interpreted from two published seismic profiles. White '+' symbols indicate contact locations as predicted from magnetic modeling.

The initial goal of this modeling project was to try to determine the contact between the carbonates outcropping on the western side of the fjord and the igneous intrusives outcropping on the eastern side. Interpretation of seismic data from a 1988 survey placed the contact near and parallel to the eastern side of the fjord. The magnetic anomaly in the center of the fjord from the 1997 NGU helicopter survey left open the possibility that the contact could be further west, near this anomaly. However, Euler deconvolution and inverse and forward modeling results support the placement of the contact near the eastern side of the fjord, and are generally consistent with the contact derived from the Noteby seismic survey (Fig. 12). Modeling also suggests that the larvikite intrusion may slant towards the east with increasing depth in the north part of the fjord, but in the vicinity of the Norcem mine the slant is westward.

Although according to these models the carbonate unit extends across the fjord, the magnetic body causing the central magnetic anomaly may extend into the carbonate unit and hinder mining operations beyond this point. L301 is the line nearest the Norcem mine, and the model of this line in Fig. 8 shows the larvikites to be very near the central fjord intrusive. The amount of extractable carbonates east of the central fjord intrusion might therefore be small.

5 ACKNOWLEDGMENTS

Andreas O. Harstad (Norcem AS) collected the 135 rock samples used for rock property studies. Anna Sommaruga (NGU) advised in the interpretation of the Noteby seismic data. Jon Mogaard (NGU) was responsible for collecting the helicopter magnetic data. Discussions with Odleiv Olesen (NGU) helped to better constrain the models and make them more geologically relevant.

6 REFERENCES

Beard, L.P., 1999: Data acquisition and processing – Helicopter geophysical surveys, Larvik, 1998. Norges geologiske undersøkelse rapport 99.026, 13 pp.

Dons, J.A. and Jorde, K., 1976: Geologisk kart over Norge – 1:250 000 Skien.

Encom, 1999: ModelVision Pro User's Guide Version 3.0. Encom Technology Pty Ltd., 113 pp.

Harstad, Andreas O., 1999: Contact metamorphism in the Porsgrunn-Eidanger aureole, S-E Norway: the effects of grain coarsening on calcite. Cand. scient. thesis, University of Oslo, 172 pp.

Marquardt, D.W., 1963: An algorithm for least-squares estimation of non-linear parameters: Journal of the Society of Industrial and Applied Mathematics 11, 431-441.

Noteby AS, 1988: Bunn- og fjellkartlegging for gruvedrift under Eidangerfjorden. Noteby rapport 44111-1, 5 pp.

Reid, A.B., Allsop, J.M., Granser, H., Millett, A.J., and Somerton, I.W., 1990: Magnetic interpretation in three dimensions using Euler deconvolution. Geophysics 55, 80-91.

APPENDIX: Rock Properties for Eidangerfjord samples (SI units)

sample	x	y	rocktype	formation	density	susceptibility	Q
C-01	534009	6550613	Granitisk-gneis	BAM	2689	0.00676	0.36611
C-02	534009	6550613	Diabas	PER	2820	0.09799	0.59587
C-03	535109	6549043	Glimmerskifer	BAM	2707	0.00016	0
C-04	535109	6549043	Amfibolitt	BAM	2990	0.01642	0.65771
C-05	535119	6548933	Kvartsitt	BAM	2662	0.00006	281.532
C-06	535739	6549103	Kvarts-	BAM	2641	0.00016	81.7071
C-07	535739	6549103	Amfibolitt/biotitt	BAM	2904	0.00473	13.8607
C-08	535739	6549103	Kvartsitt	BAM	2666	0.00617	1.46300
C-09	535739	6549103	Kvartsitt	BAM	2633	0.00054	25.7092
C-10	535739	6549103	Kvarts/sandste	BAM	2640	0.00129	11.9801
C-11	535739	6549103	Amfibolitt/biotitt	BAM	3070	0.02293	0.40713
C-12	535499	6548213	Gneis	BAM	2669	0.00038	0.19730
C-13	535559	6548173	Amfibolitt	BAM	2999	0.00224	0.19673
C-14	535849	6547193	Gneis	BAM	2651	0.00227	0.19413
C-15	535849	6547193	Gneis	BAM	2793	0.00062	0.68543
C-16	536859	6546363	Diabas	PER	2749	0.00075	0.10334
C-17	536859	6546363	Amfibolitt	BAM	3017	0.00077	9.74109
C-18	536859	6546363	Amfibolitt	BAM	2988	0.00056	0
C-19	536859	6546363	Amfibolitt	BAM	3225	0.00129	0.13768
C-20	536859	6546363	Gneis	BAM	3067	0.00063	0.12300
C-21	536959	6545713	Kvarts/sandste	BAM	2619	0.01308	0.15383
C-22	536959	6545713	Gneis	BAM	2823	0.00079	9.81116
C-23	536959	6545713	Kvartsitt-gneis	BAM	2806	0.00254	0.12720
C-24	538739	6544303	Gneis	BAM	2671	0.00018	0.61080
C-25	538749	6544243	Amfibolitt	BAM	2940	0.00049	0
C-26	538859	6547593	Kalkstein	STE	2707	0.00118	0.41545
C-27	538859	6547593	Leirskifer/kalks	FSS	2873	0.0004	0.43737
C-28	538859	6547593	Leirskifer/kalks	FSS	2894	0.00043	0
C-29	538859	6547593	Leirskifer/kalks	FSS	2880	0.00078	1.24370
C-30	538859	6547593	Leirskifer/kalks	FSS	2886	0.00032	1.92898
C-31	538859	6547593	Leirskifer/kalks	FSS	2860	0.00029	0.58597
C-32	538859	6547593	Leirskifer/kalks	FSS	2777	0.00033	0.71186
C-33	538859	6547593	Leirskifer/kalks	FSS	2893	0.00072	3.82999
C-34	538859	6547593	Leirskifer/kalks	FSS	2922	0.00067	5.86185
C-35	538859	6547593	Leirskifer/kalks	FSS	2909	0.00089	6.27376
C-36	538859	6547593	Leirskifer/kalks	FSS	2885	0.0007	5.90366
C-37	538859	6547593	Leirskifer/kalks	FSS	2886	0.00068	11.1028
C-38	538859	6547593	Leirskifer/kalks	FSS	2906	0.0016	11.7935
C-39	538859	6547593	Leirskifer/kalks	FSS	2938	0.00043	4.75460
C-40	538859	6547593	Leirskifer/kalks	FSS	2853	0.00022	1.27213
C-41	538859	6547593	Leirskifer	ELN	2777	0.00026	0
C-42	538859	6547593	Diabas	PER	3185	0.00487	10.6140
C-43	538859	6547593	Kalkstein	HUK	2747	0.00047	8.77471

C-44	538859	6547593	Diabas	PER	2968	0.01393	6.24089
C-45	538859	6547593	Alunskifer	ALU	2726	0.01457	16.7724
C-46	538859	6547593	Diabas	PER	3147	0.00517	18.0335
C-47	538859	6547593	Diabas	PER	3102	0.00348	13.1285
C-48	538859	6547593	Kvartsitt	CAM	2620	0.00001	17.4882
C-49	538859	6547593	Diabas	PER	3163	0.00092	0.22287
C-50	538859	6547593	Gneis	BAM	2748	0.00029	1.56834
C-51	539679	6546493	Skifer	VEN	2781	0.00071	0.60212
C-52	539639	6546523	Skifer	VEN	2774	0.00357	4.34934
C-53	539699	6547503	Kalk/leir+sand	HER	2826	0.00035	1.03536
C-54	539769	6547573	Klastisk-matr.	HER	2794	0.00053	2.25436
C-55	539889	6547583	Kalk/leir/sand	HER	2905	0.00069	1.79348
C-56	539869	6547823	Kalksilikat	HER	2891	0.00081	1.05260
C-57	539719	6548943	Lysegrå-b.a.	HER	2720	0.00268	1.66095
C-58	539719	6548943	Lysgrå-b.a.	HER	2802	0.00011	0.47699
C-59	539909	6549373	Lys/mørk-	SAE	2760	0.00022	0
C-60	539649	6551153	Sand/silt.b.a.	SAE	2683	0.00014	0.66035
C-61	539649	6551153	Leirholdig-b.a.	SAE	2730	0.00026	0.35561
C-62	539789	6551173	Kalkstein	RYT	2753	0.00008	4.43481
C-63	539709	6551483	Kalkstein	RYT	2732	0.00006	7.66188
C-64	539829	6551533	Kalk/leirskifer	VIK	2817	0.00021	0
C-65	539829	6551533	Kalk/leirskifer	VIK	2717	0.00037	0.29044
C-66	539889	6551613	Skarn-b.a.	VIK	3236	0.00068	0.89337
C-67	540109	6551743	Kalk/silt-b.a.	SKN	2880	0.00047	0.58498
C-68	540109	6551743	Diabas	PER	2957	0.0041	0.97098
C-69	540079	6551993	Siltstein/kalk	STF	2780	0.0001	0
C-70	540069	6552153	Leirskifer	STF	2972	0.00309	2.00724
C-71	540129	6552373	Kalkstein/silt	STF	2767	0.0007	3.78577
C-72	539339	6553043	Kalkstein	STF	2933	0.00012	0.72875
C-73	540139	6553033	Sandstein	HLM	2833	0.0002	0.38731
C-74	540139	6553033	Sandstein/leir	HLM	2753	0.00029	4.93770
C-75	540449	6553533	Sandstein	HLM	2792	0.00003	0
C-76	540449	6553533	Sandstein	HLM	2634	0.00003	8.57772
C-77	540449	6553533	Sandstein	HLM	2729	0.00038	0.48669
C-78	540659	6552733	Sandstein	HLM	2747	0.00004	2.43593
C-79	540659	6552733	Sandstein	HLM	2676	0.0001	0.84950
C-80	540929	6553503	Sandstein	HLM	2714	0.00062	0.43142
C-81	541039	6553383	Nefelinsyenitt	PER	2619	0.00654	0.21301
C-82	541039	6553383	Basalt	PER	3197	0.04201	1.98995
C-83	541039	6553383	Basalt	PER	3095	0.06964	1.26572
C-84	540819	6552453	Nefelinsyenitt	PER	2764	0.13577	0.89074
C-85	540849	6552403	Rombeporfyr	PER	2689	0.05163	0.12309
C-86	540879	6552323	Larvikitt	PER	2673	0.01601	0.22354
C-87	540919	6552983	Larvikitt	PER	2685	0.03002	9.88341
C-88	540919	6552983	Basalt	PER	3195	0.11991	3.31503
C-89	540989	6553093	Nefelinsyenitt	PER	2654	0.01849	1.09664
C-90	541059	6553213	Nefelinsyenitt	PER	2666	0.00121	0.65323

C-91	541269	6551923	Larvikitt	PER	2685	0.0177	1.44535
C-92	541269	6551923	Nefelinsyenitt	PER	2632	0.01269	0.85110
C-93	541269	6551923	Nefelinsyenitt	PER	2613	0.0117	1.57008
C-94	541139	6551063	Nefelinsyenitt	PER	2717	0.02358	1.18034
C-95	541189	6549923	Larvikitt	PER	2701	0.01809	2.23542
C-96	541199	6548983	Larvikitt	PER	2702	0.01662	1.29634
C-97	541799	6548103	Larvikitt	PER	2692	0.02676	0.70598
C-98	542999	6547993	Nefelinsyenitt	PER	2690	0.01911	1.05438
C-99	543979	6546483	Nefelinsyenitt	PER	2671	0.00906	0.86395
C-100	544389	6546153	Nefelinsyenitt	PER	2702	0.00373	1.24977
C-101	540179	6547613	Brunkalk	STE	2802	0.00013	0.80724
C-102	540179	6547613	Kalkstein	STE	2726	0.00075	3.15020
C-103	540179	6547613	Kalkstein	STE	2715	0.00004	9.24404
C-104	540179	6547613	Kalkstein	STE	2742	0.00026	2.70077
C-105	540179	6547613	Kalkstein	STE	2722	0.00001	27.4814
C-106	540179	6547613	Kalk-leirstein	STE	2790	0.00005	0.94939
C-107	541369	6547603	Larvikitt	PER	2700	0.01592	3.54165
C-108	541819	6547553	Nefelinsyenitt	PER	2663	0.01556	0.95388
C-109	542029	6547573	Larvikitt	PER	2714	0.02233	2.28986
C-110	542129	6547203	Larvikitt	PER	2722	0.00835	0.17618
C-111	542009	6546873	Larvikitt	PER	2706	0.02509	16.8397
C-.112	542419	6547083	Nefelinsyenitt	PER	2688	0.00785	0.43076
C-113	542419	6547083	Larvikitt	PER	2689	0.01994	1.14997
C-114	542479	6546613	Larvikitt	PER	2697	0.02105	1.29567
C-115	542309	6547003	Larvikitt	PER	2688	0.02107	0.43887
C-116	542429	6546263	Larvikitt	PER	2713	0.02016	1.12236
C-117	542429	6546263	Larvikitt	PER	2806	0.00072	0.63196
C-118	542429	6546263	Larvikitt/pegma	PER	2735	0.00197	0.26683
C-119	543419	6545543	Nefelinsyenitt	PER	2688	0.01436	1.29990
C-120	541769	6545573	Larvikitt	PER	2738	0.03073	1.72201
C-121	540729	6551723	Larvikitt	PER	2706	0.01021	2.32752
C-122	540729	6551723	Nefelinsyenitt	PER	2720	0.0092	2.20392
C-123	540729	6551723	Larvikitt	PER	2737	0.02794	0.45102
C-124	540729	6551723	Diabas	PER	2837	0.02487	2.08807
C-125	540919	6551853	Nefelinsyenitt	PER	2650	0.00049	0.62232
C-126	540919	6551853	Nefelinsyenitt	PER	2687	0.00121	2.14782
C-127	541309	6546553	Larvikitt	PER	2703	0.00033	0.30292
C-128	542449	6544403	Nefelinsyenitt	PER	2697	0.02933	0.34790
C-129	542449	6544403	Larvikitt	PER	2707	0.01245	0.12677
C-130	542969	6543813	Nefelinsyenitt	PER	2738	0.0007	0.17857
C-131	542969	6543813	Larvikitt	PER	2709	0.02231	2.30766
C-132	543189	6543153	Nefelinsyenitt	PER	2713	0.00453	0.21051
C-133	543189	6543153	Nefelinsyenitt	PER	2707	0.01479	0.84216
C-134	543909	6543643	Larvikitt	PER	2701	0.01611	1.40399
C-135	543889	6543723	Larvikitt	PER	2697	0.02464	1.15297

Formation name key:

HUK	Huk Formation
ELN	Elnes Formation
STE	Steinvika Formation
FSS	Fossum Formation
VEN	Venstøp Formation
HER	Herøy Formation
SAE	Sælabonn Formation
RYT	Ryttråker Formation
VIK	Vik Formation
SKN	Skinnerbukt Formation
STF	Steinsfjorden Formation
HLM	Holmestrand Formation
ALU	Alunskifer Formation
BAM	Bamle Complex
PER	Permian Igneous Province

Coordinates: UTM Zone 32N